Satellite Altimetry Applications off the Coasts of North America

16

W.J. Emery, T. Strub, R. Leben, M. Foreman, J.C. McWilliams, G. Han, C. Ladd, and H. Ueno

Contents

16.1 Background 418
16.2 East Coast of North America 419
16.2.1 The Labrador Sea and Coastal Eastern Canada 419
16.2.2 The Scotian Shelf and the North Atlantic Bight 421
16.3 The Gulf of Mexico and Caribbean Sea 425
16.4 West Coast of North America 429
16.4.1 California Current System 431
16.5 Alaskan Stream 443
16.6 Tidal Energy in the Bering Sea 447
16.7 Future Work 448
References 448

W.J. Emery (✉) and R. Leben
CCAR, University of Colorado, Boulder, CO 80309-0431, USA
e-mail: william.emery@colorado.edu

T. Strub
COAS, School of Oceanography, Oregon State University, Corvallis, OR, USA

M. Foreman
Institute of Ocean Sciences, Sidney, B.C., Canada

J.C. McWilliams
Institute of Geophysics and Planetary Physics, UCLA, Los Angeles, CA, USA

G. Han
Fisheries & Oceans Canada, Northwest Atlantic Fisheries Center, St. John's, NL, Canada

C. Ladd
Pacific Marine Environmental Lab, NOAA, Seattle, WA, USA

H. Ueno
Institute for Observational Research into Global Change, Japan Agency Marine-Earth Science and Technology, Yokosuka, Kanagawa, Japan

S. Vignudelli et al. (eds.), *Coastal Altimetry*,
DOI: 10.1007/978-3-642-12796-0_16,

Keywords Satellite altimetry • U.S. coasts • California Current • Gulf of Mexico • Gulf Stream • Labrador Current • Loop Current

Abbreviations

ADCP	Acoustic Doppler Current Profiler
AVHRR	Advanced Very High Resolution Radiometer
AVISO	Archiving, Validation and Interpretation of Satellite Oceanographic data
CHL	CHLorophyll
CTD	Conductivity-Temperature-Depth
DEM	Digital Elevation Model
DOT	Dynamic Ocean Topography
DUACS	Data Unification and Altimeter Combination System
ECMWF	European Centre for Medium-Range Weather Forecasts
EKE	Eddy Kinetic Energy
ENSO	El Niño Southern Oscillation
EOF	Empirical Orthogonal Function
GOES	Geostationary Operational Environmental Satellite
JPL	Jet Propulsion Laboratory
MCC	Maximum Cross Correlation
NCEP	National Center for Environmental Prediction
RMS	Root Mean Square
ROMS	Regional Oceanic Modeling System
SCB	Southern California Bight
SSALTO	Segment Sol multimissions d'ALTimétrie, d'Orbitographie et de localisation précise
SSH	Sea Surface Height
SSHA	Sea Surface Height Anomaly
SST	Sea Surface Temperature
TG	Tide Gauge
T/P	TOPEX/Poseidon
VACM	Vector-Averaging Current Meter
WOCE	World Ocean Circulation Experiment
XBT	eXpendable BathyThermograph

16.1 Background

A number of studies have used satellite altimeter data, alone or in combination with other satellite, in situ or model fields, to investigate the circulation of the boundary currents surrounding North America. In nearly all cases, these investigations have concentrated on the variability in the seasonal jets and mesoscale circulation features found in the several hundred kilometers next to the coast. Only recently have there been attempts

to retrieve and use altimeter sea surface height (SSH) data in the traditional domain of "coastal oceanography," over the continental shelf and/or within several tens of kilometers of land. The problems encountered off North America in retrieving altimeter data near land are the same as those described in other regions – primarily distortions of the altimetric waveforms, non-linear tidal currents over continental shelves, and a lack of atmospheric water vapor correction due to interaction of the land with the passive microwave radiometer used for this correction (Vignudelli et al. 2005). The methods used to investigate the mesoscale circulation fields in the larger-scale boundary currents have been instructive, however, in establishing the nature and limitations of traditional altimetric approaches and suggesting improvements and modifications that allow altimeter data to be extended closer to land. Here we describe those earlier altimetric studies and note how they evolved into the more coastal investigations that are now under way.

Another complexity of these coastal zones is the contribution of the ageostrophic components of the coastal currents, which cannot be mapped using satellite altimetry. The simplest of these is the surface Ekman component, which applies to both the Deep Ocean and coastal currents and may be estimated from satellite or in situ wind measurements. Unlike the open ocean, however, other ageostrophic currents induced by the wind and tides in coastal regions are often non-linear and frequently overwhelm the geostophic currents that can be mapped using altimeter data. Other non-altimetric measurements, such as drifting buoy trajectories, current meter moorings, Acoustic Doppler Current Profiler (ADCP), currents mapped by coastal radars and currents inferred from satellite imagery, are needed to resolve the often-significant ageostrophic currents in the coastal region. These then need to be combined with the altimetric estimates of the geostrophic currents (Matthews and Emery 2009).

In the following sections we review some important results of coastal altimetry studies off the coasts of North America. We begin with a brief summary of some results of studies of the East Coast of North America starting in the Labrador Sea and then moving south to Nova Scotia and then finally to the east coast of the U.S. Studies of the Gulf of Mexico are then reviewed followed by some example studies from the west coast of North America where quite a few studies of coastal altimetry have been carried out. In between there is a short review of a paper on tides in the Bering Sea. We finish up with a short section on future plans for coastal altimetry studies in this region.

16.2 East Coast of North America

16.2.1 The Labrador Sea and Coastal Eastern Canada

For reviews of the shelf, slope, and offshore boundary circulation characteristics of the NW Atlantic, see Loder et al. (1998), Boicourt et al. (1998), Townsend et al. (2006), and Lohrenz and Verity (2006). An overly simplified depiction of the circulation along the U.S. east coast north of Cape Hatteras consists of an equatorward flow of cooler and fresher

water over the wide shelf and slope, bounded on the offshore edge by a warm and salty poleward current over the continental slope. The fresh and cool water originates to the north in the Labrador Sea, augmented by coastal inputs and diminishing in strength toward the south (Loder et al. 1998). It's southward flow is driven, at least in part, by buoyancy forcing. The Gulf Stream is relatively far offshore in this region but may contribute to the poleward slope current through its influence on offshore SSH. South of Cape Hatteras, the flow over the shelf appears less organized and the Gulf Stream stays closer to the slope.

Traditional altimeter analyzes are not usually attempted over the wide shelf, where tidal motions are strong and errors in tidal models used to remove the tidal signals from altimeter data contaminates the signal. Dong and Kelly (2003) tested four tidal models over the mid-Atlantic Bight shelf and found that none succeeded in removing the tidal signal from the altimeter data. They also found no significant correlations between the altimeter-derived velocities and current meter records over the shelf (<200 m water depth), but good correlations with measured currents over the slope (water depths of 500 m and deeper). They attributed the lack of correlations over the shelf to unresolved tidal motion and restricted their altimeter analyzes to examinations of the boundary currents over the slope and farther offshore. This has been the case for all altimeter studies along the U.S. east coast, as characterized by the selection of papers summarized below.

The early study of Kelly and Gille (1990) developed a method to estimate the Gulf Stream's position, width, and strength as it crossed repeated altimeter tracks. By assuming a Gaussian shape to the velocities and an SSH shape consistent with the geostrophic relation, they were able to estimate both the temporal mean and instantaneous absolute velocity and SSH profiles from the time series of altimeter sea surface height anomalies (SSHA, with the temporal mean removed from the altimeter record at each alongtrack location). The method relies on the fact that the Gulf Stream meanders and changes position along the track over a range of distances as large as its width. This allows them to use an iterative process and least squares fit to estimate the three parameters that define the Gaussian – its center position, width, and height. Although this may seem far removed from the coast, it comes into play in examining causes for changes in the slope currents (below).

Moving upstream to the source of the cool, fresh water flowing equatorward over the shelf, Han and Tang (2001) use 6 years of TOPEX/Poseidon (T/P) altimeter data along with a WOCE hydrographic section to compute volume transports in the western Labrador Sea (Han and Tang 2001). Two ascending altimeter tracks (Fig. 16.1) were selected that overlap the WOCE hydrographic section, which was sampled repeatedly in each of the years between 1993 and 1998. The density sections for 1994 and 1996 clearly show large horizontal density gradients over the shelf break and upper slope where the traditional Labrador Current is located. These gradients decrease sharply towards the shore and deep water. To compute seasonal transports, the bottom boundary current was assumed zero by neglecting the bottom boundary layer. Over seasonal time scales the wind-driven near surface Ekman currents are small and can also be neglected. Thus, the total cumulative seasonal volume transport can be calculated by concurrent altimetric and hydrographic data. Due to the paucity of hydrographic data the instantaneous CTD sections were used instead of seasonal averages with the seasonally averaged altimeter data. Thus, spring and summer transports were then averaged to obtain a mean April to Sept. transport.

The resulting cumulative southward transports for the time series from 1993 to 1998 are presented here in Fig. 16.2 where the total transport is computed from the barotropic and

Fig. 16.1 tracks th 3,000, a also sho of the v outer li determi Tang 2(

barocl both t height corres transp years 1998 oppos annua Sea c

16.2. The S

Don annu acro

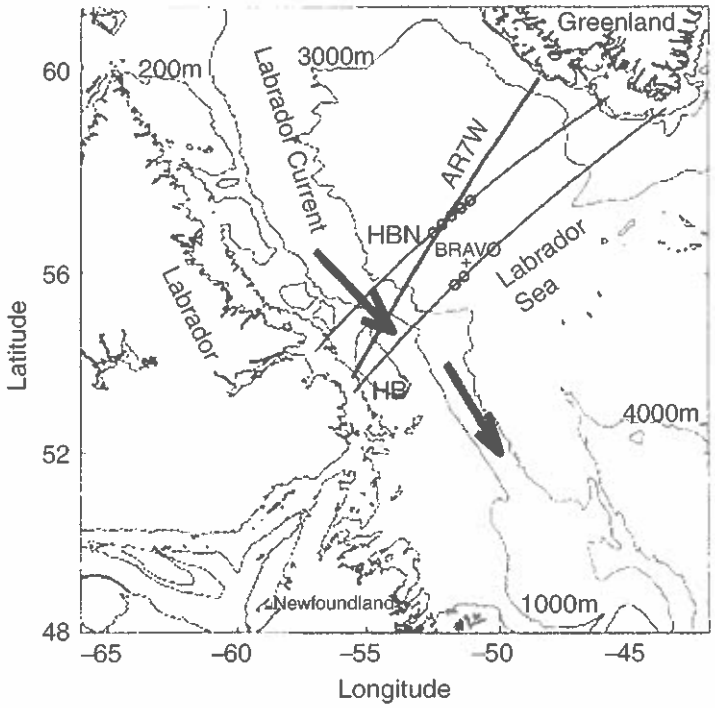

Fig. 16.1 Map showing the study area: HB and HBN are two TOPEX/Poseidon ascending ground tracks that straddled the AR7W hydrographic section in the western Labrador Sea. The 200, 1,000, 3,000, and 4,000 m isobaths (*thin lines*) and the location of the Labrador Current (*thick arrows*) are also shown. The five open circles on HBN indicate the outer limits of integration in the calculation of the volume transport, from the deepest sea westward at an interval of 25 km. The corresponding outer limits for HB (for clarity only the easternmost and westernmost locations are shown) are determined from the values of H/f (H is the water depth and f is the Coriolis parameter; Han and Tang 2001)

baroclinic components. Errors in the barotropic component were computed from errors in both the altimeter surface height anomaly and the WOCE hydrographic section dynamic height. Baroclinic errors are computed from the hydrographic data. Here a positive anomaly corresponds to a larger than average southward transport. The interannual range of the total transport is about 6.2 Sv, which is comparable to the seasonal change of about 10 Sv. The years 1993, 94, 95, and 1997 have larger than average transports while the years 1996 and 1998 have smaller than average transports. The barotropic and baroclinic transports behave oppositely, compensating for each other and resulting in a total transport anomaly with interannual variations smaller than either of the two components. The total transport in the Labrador Sea circulation is positively correlated with the winter North Atlantic Oscillation index.

16.2.2 The Scotian Shelf and the North Atlantic Bight

Dong and Kelly (2003) made use of the above results in their analysis of seasonal and interannual variability in SSHA and corresponding cross-track geostrophic velocity anomalies across six T/P tracks in the mid-Atlantic Bight (~37°–43°N) during 6 years (~1993–1998).

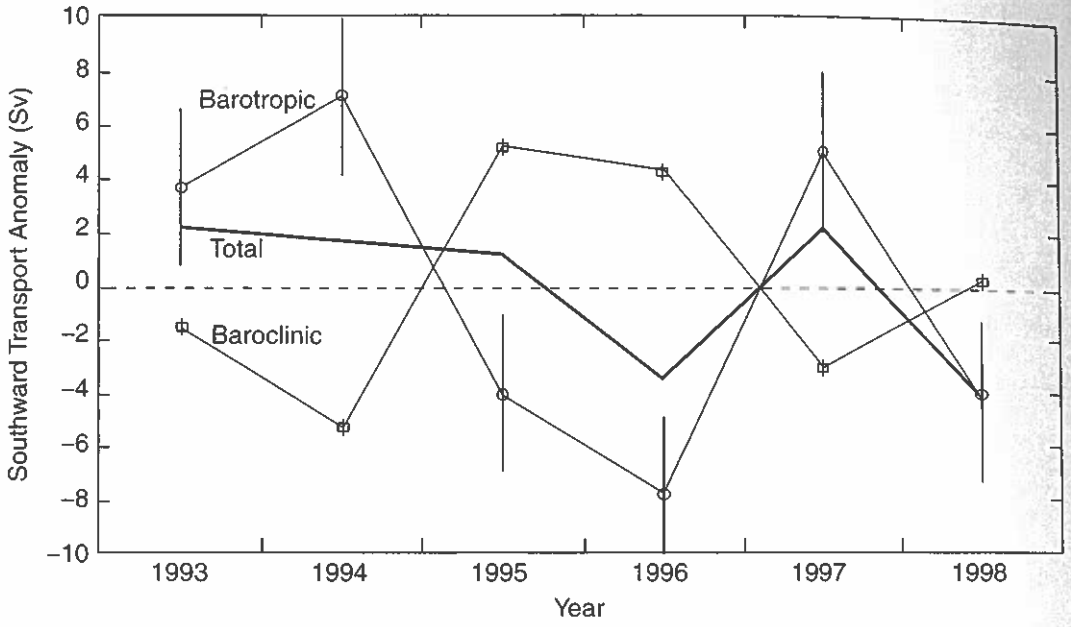

Fig. 16.2 Cumulative southward transport anomaly in the western Labrador Sea (west of the open circles in Fig. 16.1) as a function of year. The total transport (*thick lines*) is the sum of the barotropic (*circles*) and baroclinic (*squares*) components. The standard errors associated with the barotropic and baroclinic components are shown as vertical lines (Han and Tang 2001)

Their results show a seasonal reversal of the coherent southwestward surface currents along the continental slope, flowing to the northeast during the summer. A shorter record of current meters verified this reversal. During the summer of 1996, however, flow to the southwest strengthened rather than reversed. Comparisons to the strength of the outflow from the Labrador Sea (Han and Tang 2001) do not explain this anomalous behavior. Using the method of Kelly and Gille (1990), however, Dong and Kelly (2003) demonstrate that the Gulf Sream moved to the south in 1996 and they attribute the lack of northeastward flow to this shift in Gulf Stream location and lower offshore SSHA values during summer 2006, reducing the cross-slope pressure gradient and the associated along-slope geostrophic current.

Slightly farther upstream, Han (2004) analyzed a longer time series (through 2000) of T/P altimeter sea levels in conjunction with frontal analysis from infrared satellite imagery to study the temporal and spatial variability of sea-surface currents over the Scotian Slope. Geostrophic surface current anomalies normal to altimeter ground tracks are derived from sea level anomalies relative to local temporal means for the study period between 1992 and 2000. The variability of these geostrophic currents is plotted along the altimeter tracks in Fig. 16.3 as thick grey lines. Also plotted are the positions of the shelf slope front (thick dashed line) and the northern edge of the Gulf Stream (thick dash dot line). The geostrophic current anomaly including the Han et al. (1997) model mean is shown as darker, thinner lines inside the lines of geostrophic current anomaly variability.

In general, the RMS values increase westward and offshore. On individual tracks, values at the shelf break are large relative to the ones just farther offshore. The westward intensification is more evident over the western Scotian Slope and the offshore enhancement occurs mainly between the shelf-slope front and the Gulf Stream northern boundary. Typical

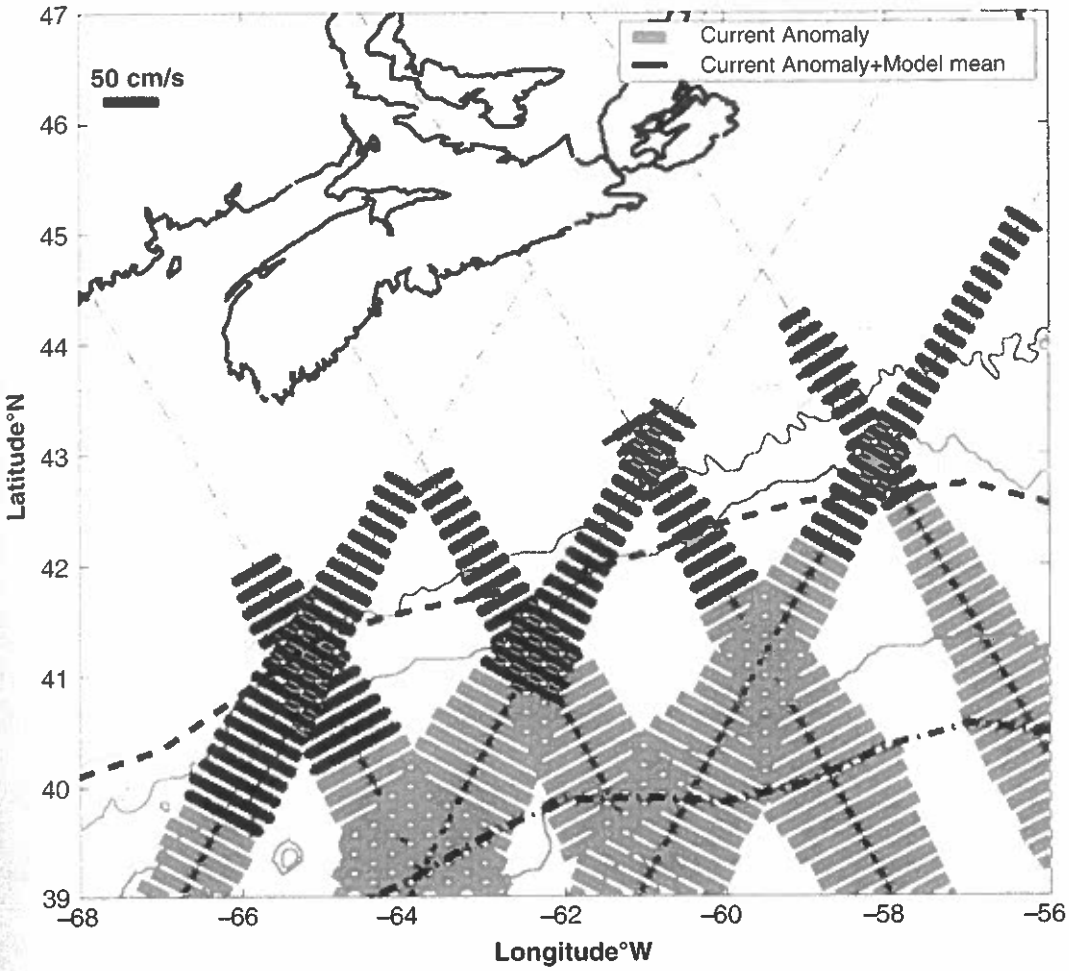

Fig. 16.3 Twice RMS values of the altimetric geostrophic current anomalies (subsampled spatially) from 1992 to 2000 (thick gray lines). The thin darker lines represent twice the RMS values when Han et al.'s (1997) model means are included. Also depicted are the positions of the shelf-slope front (*thick dashed line*) and the northern boundary of the Gulf Stream (*thick dashed dot line*; Han et al. 1997)

RMS values of the cross-track current anomalies are 20–30 cm/s over the upper and lower slope and 20–50 cm/s over the continental rise. The maximum cross-track current variability of 70–75 cm/s is located close to the Gulf Stream northern boundary. The offshore intensification is associated with the proximity of the Gulf Stream. Also, Gulf Stream rings are known to be important to the slope water circulation variability. Part of the westward intensification may also be attributed to increased warm core ring activity to the west. Crossover analyzes of altimetric current anomalies indicate that the total current variability can be estimated by a factor of 1.5 from the cross-track current variability and the variance is isotropic to within 14 %. The rotational speed of the Gulf Stream rings can reach 1–2 m/s over the Scotian Slope, with the RMS variability of ~60 cm/s.

Han (2007) extended his earlier study and that of Dong and Kelly (2003) to cover the period from 1992–2002, combining T/P geostrophic surface current anomalies with a climatological mean circulation field of a finite element model to construct nominal absolute

currents over the Scotian Slope. In Fig. 16.4 we present the annual mean climatological currents interpolated onto the satellite ground tracks. These show an equatorward flow along the shelf edge and the upper continental slope. The crossover point of the ascending and descending tracks is the only location where we can estimate the total currents from altimetry alone. These points are also shown on Fig. 16.5 as yellow spots.

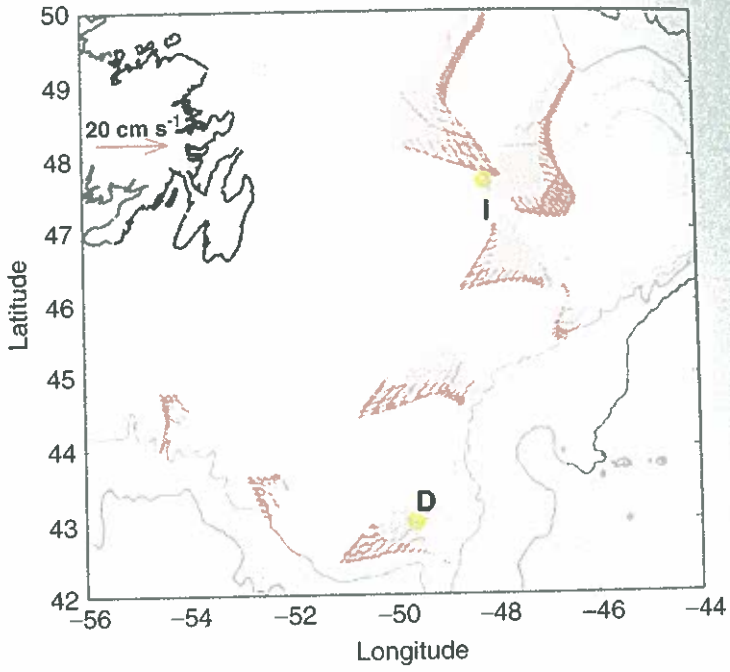

Fig. 16.4 Climatological annual mean surface currents over the Newfoundland Slope derived from Han's (2004) model results. On cross-track components are shown. The yellow point I (47.67°N, 48.19°W) and D (42.99°N, 49.60°W) represent particular crossover points of the satellite tracks (Han 2007)

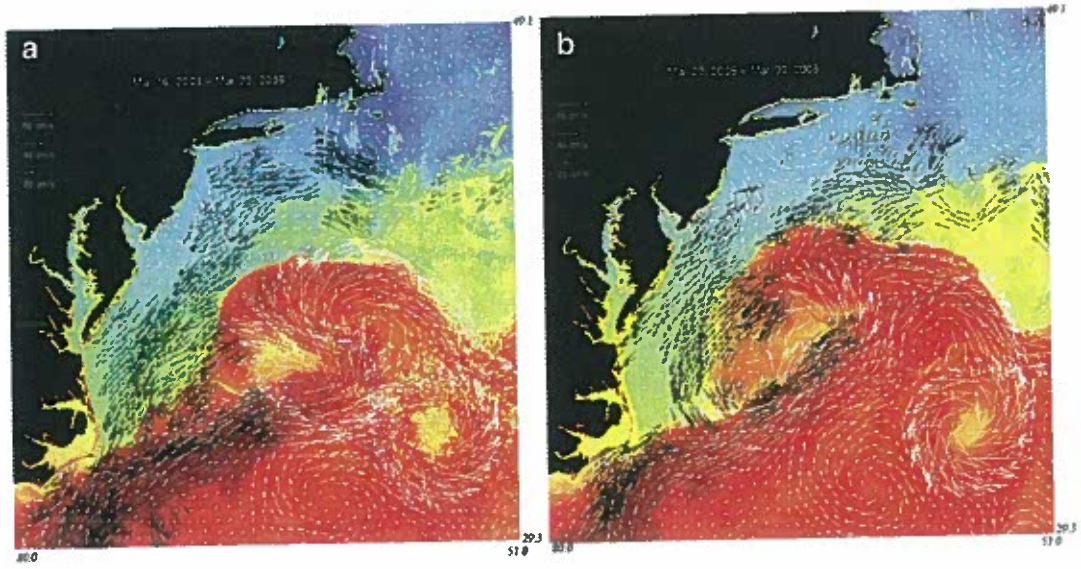

Fig. 16.5 (**a**) Week-long (Mar. 16–Mar. 23, 2008) composites of MCC currents (*black*) using both infrared and ocean color imagery and average satellite altimeter geostrophic currents (*white*) from all available altimeter satellites. (**b**)Week-long (Mar. 23–Mar. 30, 2008) composites of MCC currents (*black*) using both infrared and ocean color imagery and average satellite altimeter geostrophic currents (*white*) from all available altimeter satellites

atological
ward flow
ascending
ents from

16 –44

) using both
(*white*) from
of MCC cur-
timeter geo-

The authors of the papers cited above use along-track altimeter data and are careful not to extend that data over the shelf. Groups such as the AVISO (Archiving, Validation, and Interpretation of Satellite Oceanographic data) project now make globally gridded SSH and geostrophic velocity fields available, combining data from multiple altimeters, as described by Le Traon et al. (2003). These fields often extend into coastal regions where the alongtrack SSH data have been flagged as unreliable, for several reasons (unresolved tides, poor tracking, and wet troposphere corrections). As such, they represent extrapolated values of SSH and velocity, which have been shown off the U.S. west coast to have no significant correlation to currents measured by current meters (Saraceno et al. 2008). On a wide continental shelf such as found in West Florida and the Gulf of Mexico the gridded AVISO SSH has been shown to be a good estimate of SSH seaward of the 50 m isobath (approximately 100 km from shore; Liu and Weisberg 2007).

To examine coastal currents over shallow shelves or where land interferes with the SSH signals and their corrections, altimeter surface velocity fields must be combined with current information derived from other sources. The primary method for the calculation of surface velocities from satellite data other than altimeters is to use sequences of surface temperature or color images, either tracking small scale features using the "maximum cross correlation" (MCC) technique (Emery et al. 1986) or inverting equations for the conservation of heat to solve for the advective term (Kelly 1989) in SST image sequences. Both these methods produce similar fields and can be formally combined with altimeter cross-track velocities (Kelly and Strub 1992).

To demonstrate the information contributed by each technique, detailed maps of the mean-weekly upper ocean circulation are computed from the altimeter heights and from composites of MCC currents (black vectors) for weekly time periods. In Fig.16.5a and b two week-long surface vector fields from MCC and altimetry depicting the circulation just east of Chesapeake Bay are represented by white vectors, corresponding to the geostrophic altimeter currents, and black vectors, representing the total current estimated from sequential infrared and ocean color imagery. The black and white vectors agree well in the core regions of the northeastward flowing Gulf Stream, which splits into counter-rotating vortices. In the northern section of the cyclonic eddy that is being created to the north of the Gulf Stream, currents in both fields agree in flowing toward the southwest. Currents in the MCC field (black arrows) extend coherently over the wide shelf to the coast. The altimeter velocities, however, are more confused in the region next to the coast. Much work remains to be done in developing methods that make use of information from multiple sources in deriving optimal velocity fields over the wide shelves off the U. S. east coast.

16.3 The Gulf of Mexico and Caribbean Sea

The general circulation in the Gulf of Mexico and Caribbean Sea (sometimes called the Intra-Americas Sea) is described in reviews by Boicourt et al. (1998), Mooers and Maul (1998), and Lohrenz and Verity (2006). The topography includes a number of basins, separated by sills and shelves, and numerous islands. The primary circulation consists of water

entering in the southeast from South America to Puerto Rico, continuing west through the Caribbean Sea and then north through the Strait of Yucatan into the Gulf of Mexico, where it forms the anticyclonic Loop Current and exits the Gulf through the Strait of Florida. East of the Mississippi outflow the currents along the wide northern Gulf and Florida Shelves are generally to the east and south around Florida; west of the Mississippi outfall they are toward the west. This is again, a greatly oversimplified picture.

Altimetry in the Gulf of Mexico, as off the U.S. east coast, has not been used to map the currents over the wide shelf. In the open ocean, however, altimetric measurements offer a unique satellite capability of monitoring the strong mesoscale circulations during periods of time when infrared and ocean color surface signatures are masked by the shallow layer that responds more directly to solar insolation and thus masks the circulation driven patterns just beneath it. The microwave radar character of the satellite altimetry makes it ideal for mapping strong surface meanders such as the Loop Current, which dominates the Gulf of Mexico upper layer circulation. The Loop Current pinches off eddies that impact the shelf currents in the northwest corner of the Gulf of Mexico; the Loop Current itself can sometimes (though rarely) impact the northern Gulf shelf.

Leben (2005) developed metrics to describe the Loop Current intrusions into the Gulf of Mexico and to quantify the eddy separation for the period from Jan. 1, 1993 through July 1, 2004. Time series of Loop Current statistics such as extent, boundary length, area, circulation, and volume are found by tracking the 17-cm contour in the daily surface height maps. This contour closely tracks the edge of the high-velocity core of the Loop Current (Fig. 16.6).

This altimetric Loop Current tracking is both qualitatively and quantitatively evaluated by direct comparisons with Loop Current thermal fronts observed in sea surface temperature imagery during times of good thermal contrast and cloud-free conditions. Eddy separation events (Fig. 16.7) are identified by the changes in the Loop Current length associated with the breaking of the tracking contour.

A total of 16 Loop Current eddies generated by the Loop Current over this 11.5-year period led to significant changes in the Loop Current extent during this same period of time. Statistical and spectral analyzes indicate that eddy separation occurs most frequently at 6, 9, and 11.5 months, with little or no power at the annual frequency. Significant low frequency spectral power is found at a period of 17 to 22 months, which is associated with a far southern retreat of the Loop Current and separation periods near 18 months.

A bimodal distribution of the retreat after eddy separation is identified that influences the duration period. When the Loop Current retreats below 25°N the average separation period following retreat is 16.2 months, much longer than the 5.5 month average for the cases where part of the Loop Current remains north of 25°N. Of greater interest is the near linear relationship between the Loop Current retreat and subsequent separation periods. Thus, the irregular retreat of the Loop Current after separation may be linked to why the Loop Current exhibits such an irregular eddy separation period. In a similar study of eddy variability farther south, Carton and Chao (1999) analyzed three years of T/P altimeter SSH anomalies in the Caribbean Sea. Large cyclonic and anticyclonic eddies were found and shown to be quite regular appearing at nearly 3-month intervals west of the southern Lesser Antilles. An example shown here in Fig. 16.8 compares the mid-January 1993 SSH anomalies from T/P with coincident SSH observed by the ERS-1 satellite altimeter.

Fig. 16.6 Con
Mar. 13, 20(
same day (cc
Loop Curren
the Loop Cu

Here the
increased s
distribution
bears some

Many of
first appear
the model
above, witl
clearly sho
anomaly va
even more
age propag

Off the
absolute SS
hydrograph
This methc
brated or c

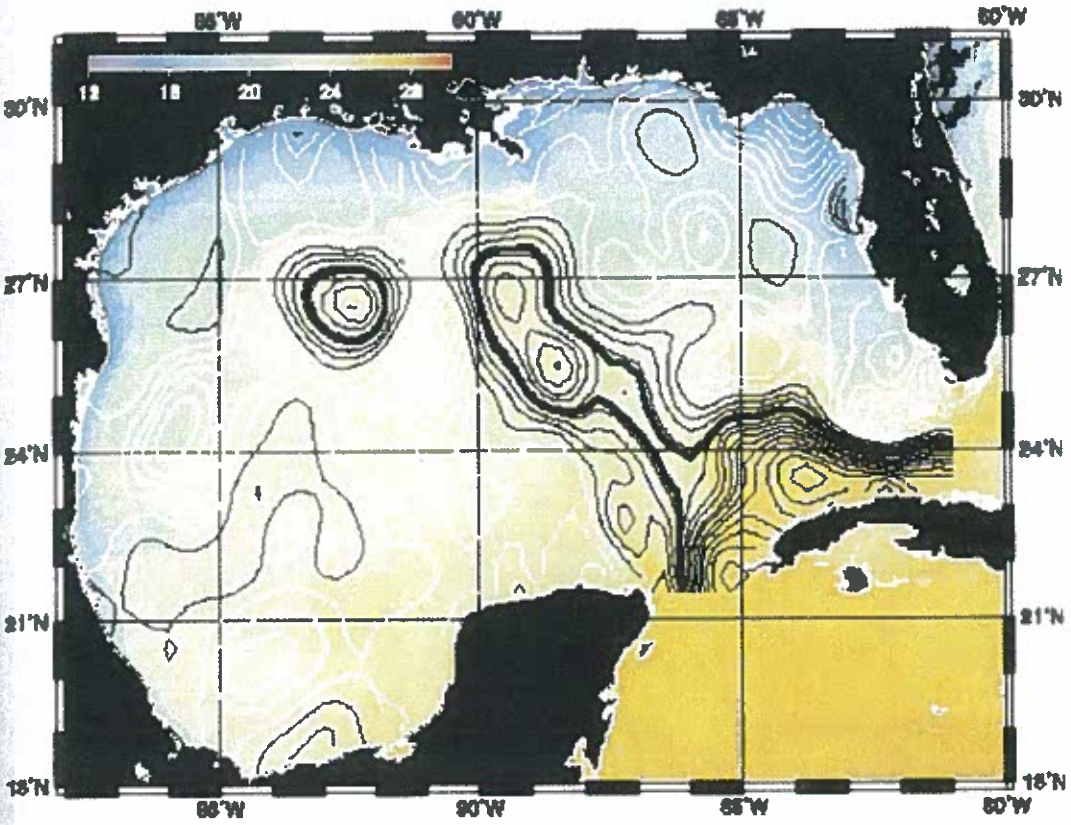

Fig. 16.6 Contoured sea surface height (*white* is negative, *black* is positive) from the altimetry map for Mar. 13, 2002 overlaid on the night-time composite SST image from the GOES 8 satellite for the same day (courtesy of Nan Walker, Louisiana State University). The 17-cm contour used to track the Loop Current boundary and eddies is shown by the bold line. The westernmost eddy separated from the Loop Current on Feb. 28, followed closely by a second eddy on Mar. 15 (Leben 2005)

Here the eddy sizes and locations are similar in both altimeters but the ERS-1 with its increased spatial resolution has eddy amplitudes that are increased by a factor of 2. The distribution of sea levels simulated by a 1/6° general circulation numerical model also bears some similarities to the T/P observations in structure but with increased amplitudes.

Many of these eddies dissipate in the coastal waters off Nicaragua half a year after they first appear. This life cycle is well reproduced in the general circulation model. Analysis of the model output suggests that these eddies are mainly limited to the thermocline and above, with little phase lag in the vertical. The westward propagation of these eddies is clearly shown in the Hovemueller diagram of Fig. 16.9. East of the Caribbean Sea level, anomaly variations are primarily annual; but within the Caribbean the sea level field is even more strongly dominated by westward propagating eddies than observed. The average propagation speed is 12 cm/s with typical spatial scales of 200–300 km.

Off the West Florida coast Liu and Weisberg (2007) proposed a method to estimate absolute SSH near the coast by integrating in situ coastal ocean observations (currents, hydrography, bottom pressure, coastal sea level, and winds) along an across-shelf transect. This method provides an independent coast SSH estimate to directly compare with calibrated or corrected coastal altimeter data. Based on a 3-year (1998–2001) time series

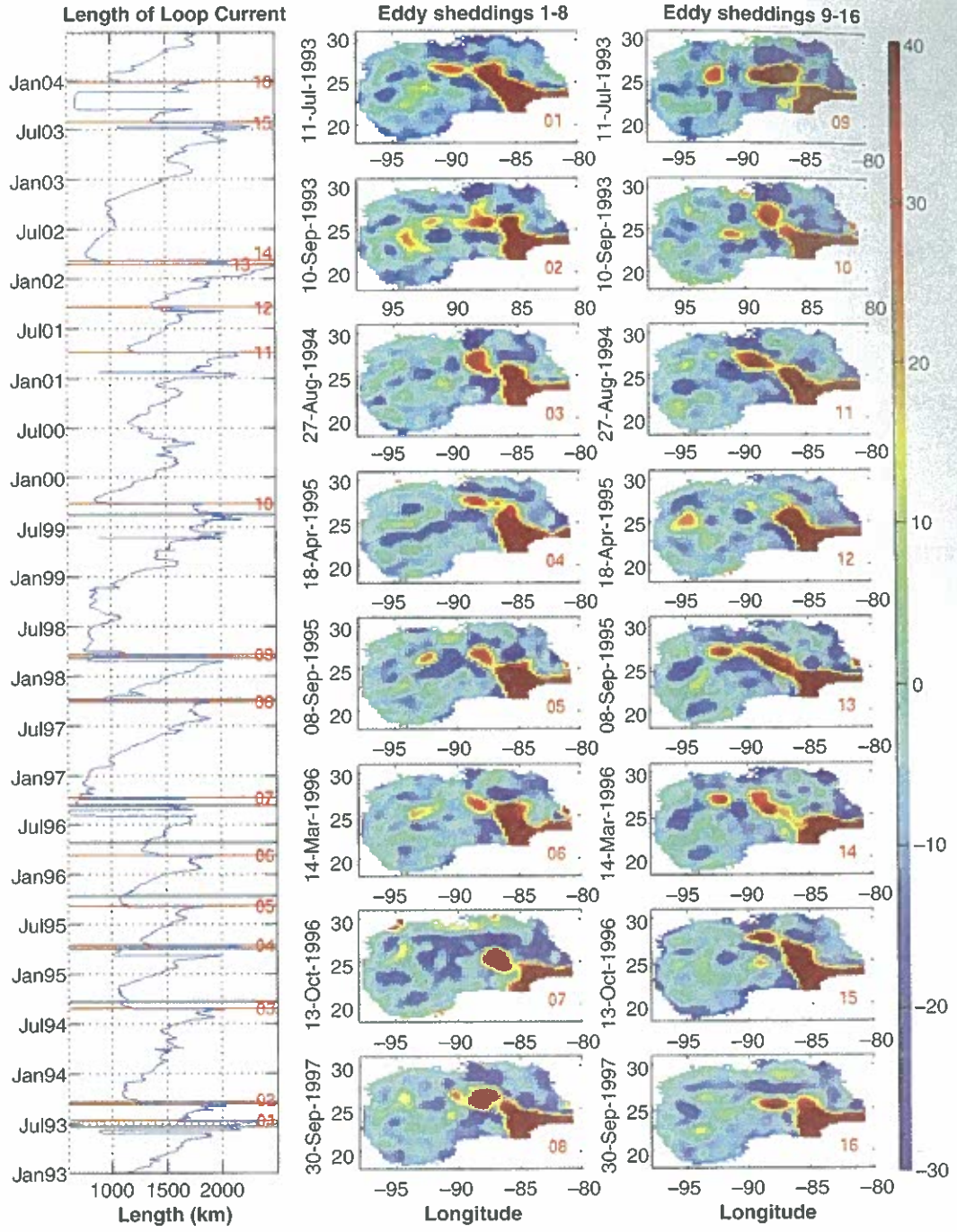

Fig. 16.7 The 16 Loop Current eddy separation events identified in the altimeter record are presented here. Sea surface height maps on the separation dates are shown in the panels to the right (note that the values above 40 cm and below −30 cm have been clipped). Eddy separation times were objectively determined by breaking of the 17-cm tracking contour, which causes a discrete change in the Loop Current length (*left panel*). The length time series is overlaid with red lines corresponding to the 16 events (Leben 2005). Gray lines show the ten separation times determined using the subjective method described in Sturges and Leben (2000)

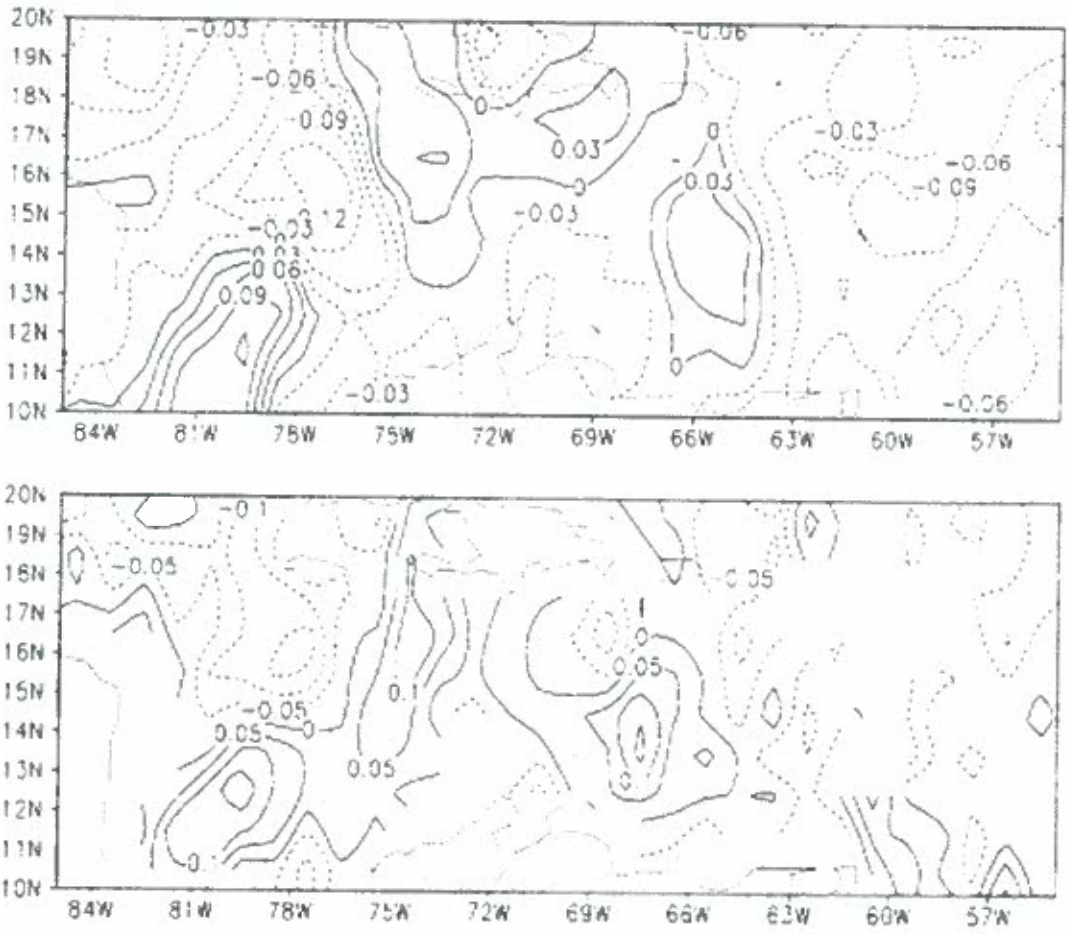

Fig. 16.8 Sea level anomaly in mid-January, 1993 as observed by T/P (*top*) and ERS-1 (*bottom*, Carton and Chao 1999)

comparison between satellite measured and dynamically estimated SST, this method appears to work well.

16.4 West Coast of North America

Circulation along the west coast of North America is summarized in reviews by Hickey (1998), Mackas et al. (2006), Royer (1998), Stabeno et al. (1998), and Badan-Dangon (1998). At the largest scales, the eastward North Pacific Current bifurcates offshore of the coast near 50°N, flowing into the poleward Alaska Current to the north and the equatorward California Current to the south. The California Current eventually turns westward off Mexico. Seasonal reversals also occur in the California Current, with poleward currents next to the coast in fall and winter. A cyclonic gyre often occupies the Southern California Bight, while the core of the California Current flows south along the western edge of the Bight. To the south of the California Current, a boundary current flows along Central

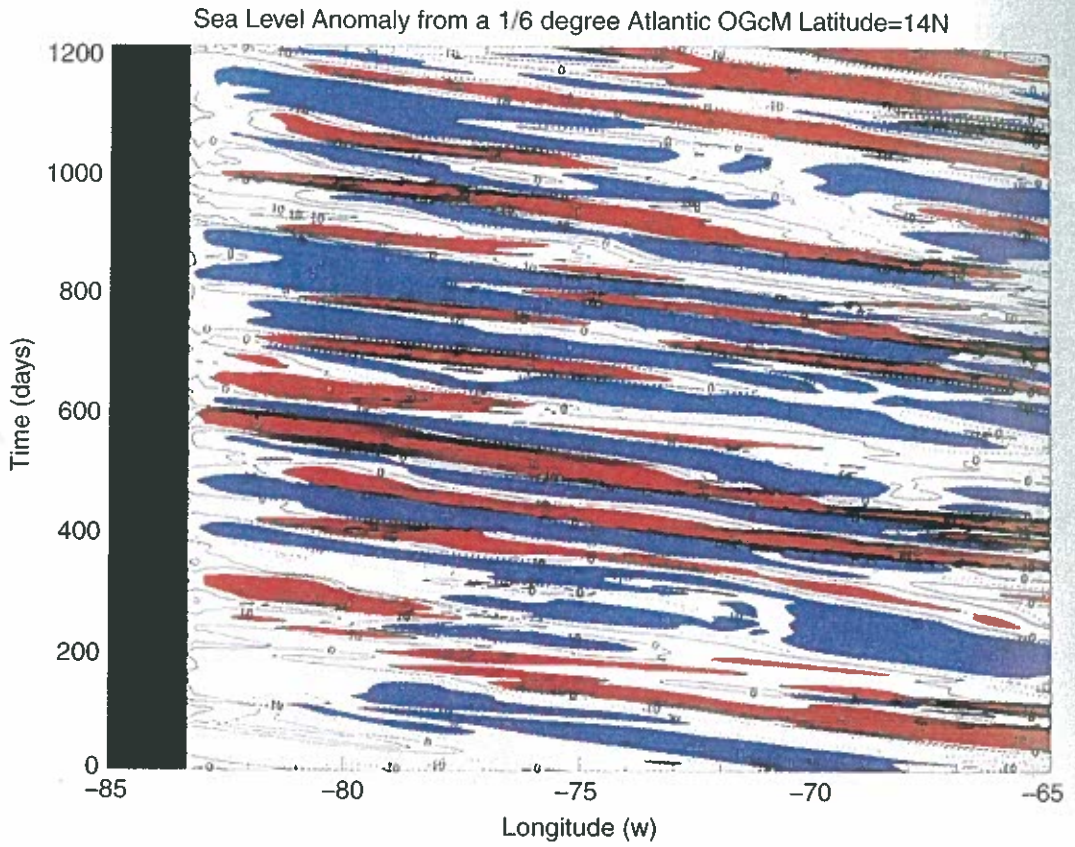

Fig. 16.9 Hovmueller diagram of simulated sea level with longitude and time at 14°N. Contour interval is 5 cm. Anomalies exceeding 10 cm are shaded (Carton and Chao 1999)

America and mainland Mexico, sometimes called the Costa Rica Current, with seasonal reversals that have not been systematically studied.

As for the U.S. east and Gulf coasts, altimetric studies have primarily looked at the mesoscale structure of currents and eddies in the core of the California Current, west of the continental shelf. Unlike the east and Gulf coasts, however, this shelf is narrow (20–50 km), allowing altimetric measurements to approach the traditional "coastal" zone. Recent investigations have attempted to push even closer to the coast, as described below.

The earliest altimetric studies used Geosat altimeter data to describe westward propagation of SSH signals in terms of annual Rossby Waves (White et al. 1990). Although these results were somewhat uncertain, due to the aliasing properties of the Geosat sampling, westward propagation of signals in the California Current has been demonstrated by numerous studies using T/P altimeter and in situ data, as well as by numerical models (Kelly et al. 1998; Strub and James 2000; Haney et al. 2001; Marchesiello et al. 2003). These signals originate next to the coast due to the annual change in the alongshore winds. Thus along the U.S. west coast, the annual and interannual variability in the coastal currents and water mass properties are transferred westward, into the deep ocean (Chereskin et al. 2000). This is unlike the east and Gulf coasts of North America, where open ocean currents and eddies may move onshore and affect the coastal circulation. Altimeter data played a key role in clarifying this aspect of coastal circulation along the west coast, as described below.

–65

'N. Contour

th seasonal

oked at the
west of the
20–50 km).
ecent inves-

rd propaga-
ough these
t sampling,
l by numer-
Kelly et al.
ese signals
as along the
; and water
2000). This
, and eddies
key role in
elow.

16.4.1
California Current System

The ability of along-track data from precision altimeters to resolve mesoscale SSH and surface velocity features in the California Current was evaluated by Strub et al. (1997) using a cluster of current meters, moored under an offshore crossover of the T/P satellite tracks. An ADCP was located directly under the crossover, while four vector-averaging current meters (VACM's) were located 2 km east and 15 km north, west, and south of the crossover. In addition, infrared satellite imagery from the Advanced Very High Resolution Radiometer (AVHRR) provided surface temperature fields that helped to interpret cross-track altimeter velocities and quantified the resolution of along-track SSH gradients.

Fig. 16.10 (left) shows geostrophic cross-track velocities along T/P tracks from one 10-day cycle, overlaid on an SST image from the same period. Extensive field surveys demonstrate that a coherent equatorward jet is found along the outer boundary of the cold water filaments and this jet is captured by the altimeter velocities, wherever the tracks cross that boundary. Because the SST features are composed of recently upwelled water, the colder temperatures indicate denser water, with lower dynamic heights. Using this relation, Strub et al. (1997) compare along-track SSH data to nearly coincident AVHRR SST data and conclude that the altimeter is capable of resolving SSH features with horizontal scales of 50–80 km in the along- track direction.

Comparing the geostrophic vector velocities from the altimeter at the cross-over at approximately 37.1°N, 127.6°W with the coincident ADCP and surrounding VACM currents leads to the following conclusions: (1) Ageostrophic Ekman currents (discussed further below) contribute to the measured currents above 48 m; (2) RMS differences of about 7–8 cm/s are found between the altimeter and ADCP measurements at 48 m; (3) Much of the RMS velocity difference comes from unresolved small-scale (15–30 km) variability in the oceanic currents – the altimeter velocities are more similar to spatially averaged (over the cluster) currents, with an RMS magnitude of 3–5 cm/s or less between the altimeter and spatially averaged current meter velocities; and (4) variance ellipses calculated from the altimeter velocities at the cross-over are in good agreement with those calculated from the subsampled current meter. The third point is consistent with the fact that a 62 km length scale is used to calculate the SSH gradient in the geostrophic altimeter velocity calculation.

These analyzes established confidence in the ability of the T/P altimeter to sample the SSH and velocity field in the California Current system. In addition, variance ellipses calculated over the entire California Current demonstrate that the velocity components are not isotropic but are polarized and that the energetic region of the California Current is surrounded and isolated by a region of lower energy (an "eddy desert") starting 500–700 km offshore. This provides evidence that the dominant energy within about 500 km of the coast is not brought into the region from a deep-ocean eddy field to the west, but must be generated within the California Current.

Adding fields of gridded SSH to the along-track data analyzes, Strub and James (2000) describe the seasonal cycle of SSH, currents and eddy statistics off the west coast of the U.S. and Baja California, extending the region considered to include the eastern North Pacific between the Equator and the Gulf of Alaska (Fig. 16.11). These studies build on an earlier look at gridded SSH fields using Geosat data from 1987 and 1988 (Strub and James 1995).

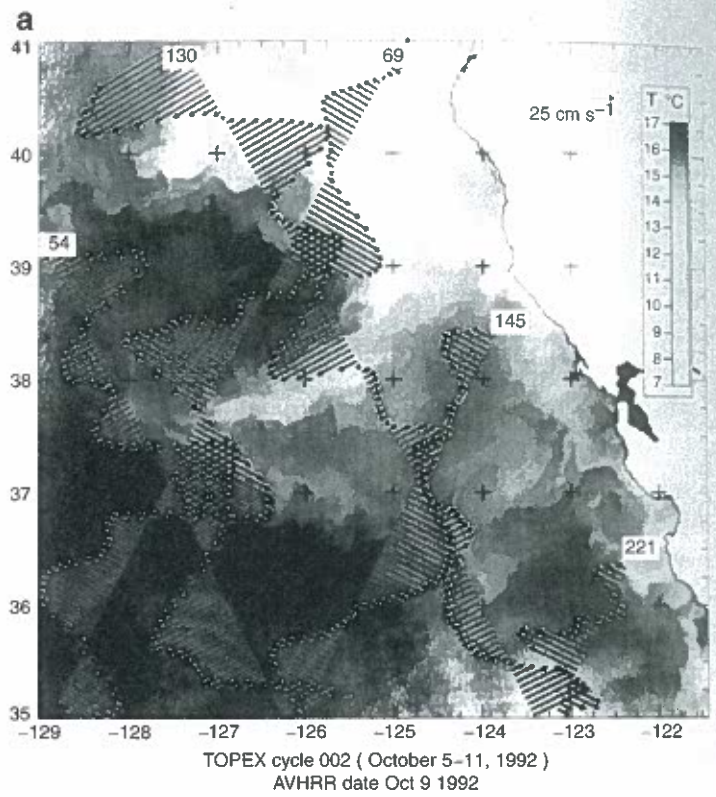

Fig. 16.10 (**a**) A field of T/P cross-track velocities from cycle 2 (October 5–11, 1992), characteristic of late summer and fall, overlain on an SST image from October 9, 1992. The current meter moorings are located under the crossover of tracks 54 and 69. (**b**) SSH contours from a combination of altimeter (T/P and ERS-1) and tide gauge data, centered on August 27, 1993 and overlaid on an AVHRR SST image from the same day. Four tide gauges are used, located at approximately 40.8°, 39.0°, 38.0°, and 36.6°N (Strub et al. 1997)

Fig. 16.11 T
indicate th
tional to th

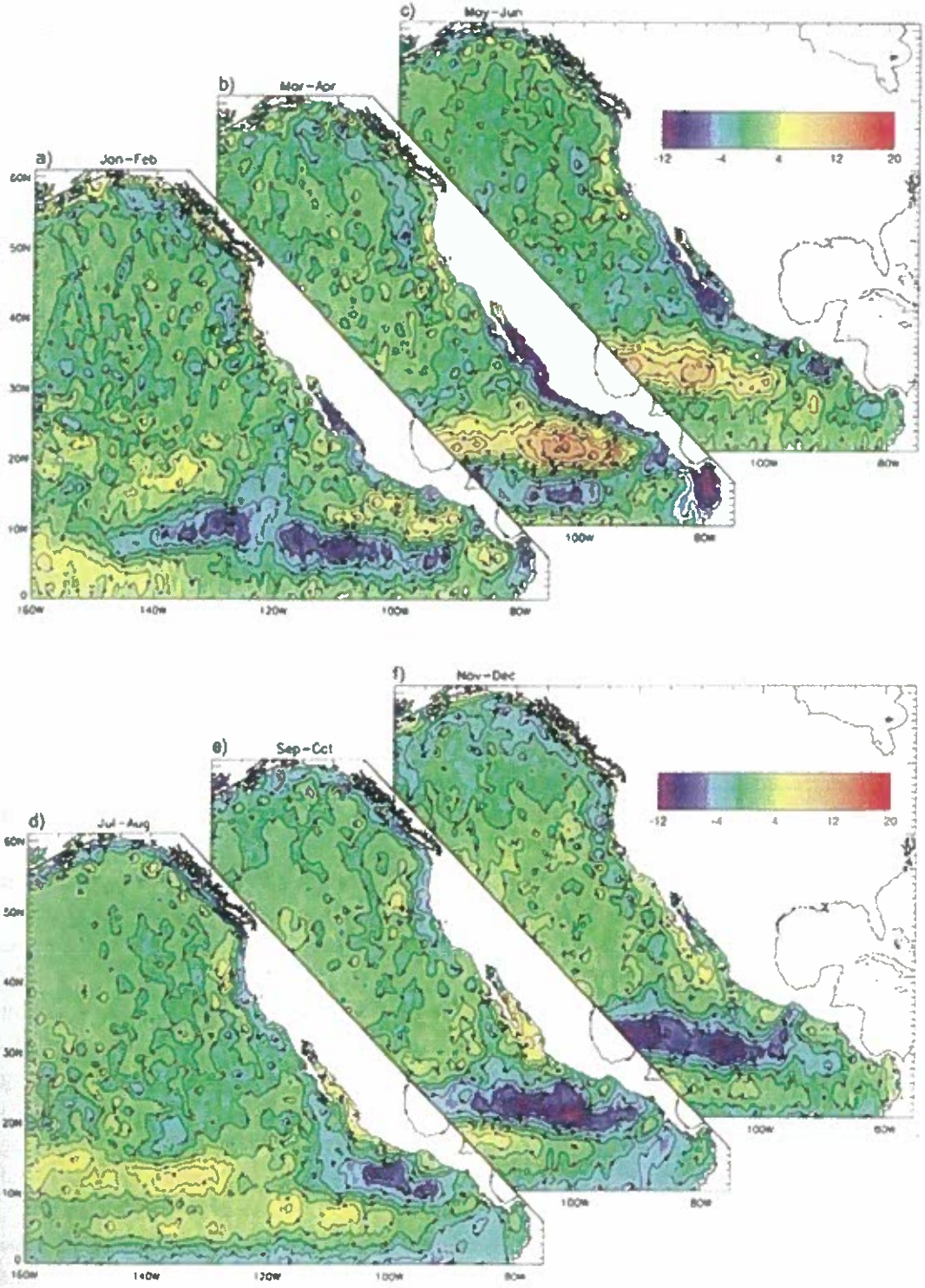

Fig. 16.11 Two-month seasonal SSH residuals based on Geosat, T/P, ERS-1, and ERS-2. Arrows indicate the direction of geostrophic flow and geostrophic surface transports are inversely proportional to the contour spacing. The contour interval is 2 cm (Strub and James 2002a)

Those fields demonstrated that the summer filaments and jets sampled off central California by numerous studies are part of a continuous jet extending from Washington to Southern California; they did not, however, establish the origin of that jet.

The later studies (Strub and James 2000, 2002a) use SSH data from a combination of multiple altimeters (Geosat, T/P and ERS-1) and tide gauges (TG), which allow the gridded SSH fields and alongshore transports to extend to the coast, bridging the traditional coastal gap in altimeter data. In these fields, the dominant variability in SSH and transport north of 20°N occurs along the boundaries, within several hundred kilometers of the coast. The eastward North Pacific Current is found to vary only weakly on seasonal time scales. Bograd et al. (1999) found a weak increase of flow in the North Pacific Current in winter on the basis of drifting buoy velocities, but this seasonal change was much weaker than the variations found in the boundary currents of the California Current System, consistent with the analysis of Strub and James (2002a).

The large-scale SSH fields along the U.S. West Coast clarify that the alongshore bands of high and low SSH form next to the coast, driven by seasonal downwelling- and upwelling-favorable winds, then move westward. Wave number spectra are useful in tracking the larger scales of the meanders formed near the coast as they move westward into the deep ocean, where the ambient spatial scales are smaller. Previous studies using drifter and altimeter data (Kelley et al. 1998) also document the offshore seasonal movement of eddy kinetic energy (EKE) generated in the vicinity of the seasonal jet. Interannual variability of the EKE field has been studied using wavelet analysis by Keister and Strub (2008). Although they could analyze details of the EKE field in the middle of California Current, 100–400 km from the coast, they could not look within the 100 km closest to the coast to verify the origin of the EKE in the very nearshore jets that form each year. However, combined with the appearance of the "eddy desert" farther offshore, the westward propagation of signals points to the seasonally developing coastal jet as the source of eddy energy in the mesoscale field of the California Current. A similar development, with different timing, occurs in the Gulf of Alaska, where the nearshore EKE is strongest in winter, moving offshore in summer. This implies that the EKE is generated in the poleward Alaska Current and Alaska Stream, which are strongest in winter next to the northern and northeastern boundary of the Gulf of Alaska.

The larger-scale fields of SSH in Strub and James (2002a) also demonstrate a coherent seasonal evolution of low and high coastal SSH signals that move from low to high latitudes around the basin. Low SSH values occur next to the coast off Central America during boreal winter, while coastal SSH values are high north of 30°N, from southern California to the Gulf of Alaska. These signals move counter-clockwise around the basin, reversing the fields by boreal summer, roughly following the expanding and contracting high and low pressure systems in the North Pacific atmospheric patterns.

The innovation in the above investigations is the use of tide gauge data to span the coastal gap in altimeter data. The same procedure was used in a subsequent study of the residual transports between the deep ocean and the coast of Oregon, Washington, and British Columbia during the 2000–2002 period, using T/P data (Strub and James 2003). Anomalous eastward transports into the boundary region along British Columbia between 52° and 54°N occurred first, between mid-2000 to mid-2001, followed by eastward transport into the boundary between 50° and 52°N in 2001. At the same time, anomalous transports were southward in the 300 km closest to the coast from 2000–2002, strongest in 2001 and the first half of 2002. These altimeter-derived transports suggest that both onshore and

southward
tributed to
supports t
onshore ac
in the pyc
found a s
California
2002. If th
km south

In anot
of the Nor
fields usin
perature, s
were calcu
The mean
field is sh
Compa
(incorpora

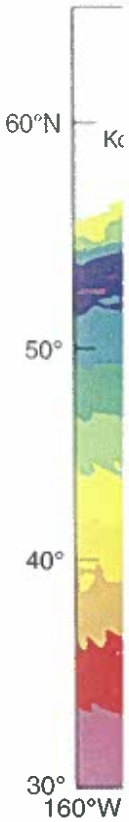

Fig. 16.12 A
ity climat
square at t
3.15 cm (I

southward displacement anomalies off British Columbia and the Pacific Northwest contributed to the subarctic characteristics of the water observed off Oregon in this event. This supports the conclusions of Freeland et al. (2003) regarding the equatorward and/or onshore advection of subarctic water that created the cold, fresh, and rich anomalies found in the pycnocline off the Pacific Northwest in summer of 2002. Bograd and Lynn (2003) found a similar (fresh, cold and nutrient-rich) subsurface anomaly in the core of the California Current (150–350 km offshore) off southern California (33°–35°N) in summer 2002. If the anomaly reported by Freeland et al. (2003) at 50°N in mid-2001 moved 1,500 km south in 1 year, it would account for the Bograd and Lynn observations.

In another large-scale study with implications for the coastal currents in the boundaries of the North Pacific, Foreman et al. (2008) calculated dynamic ocean topography (DOT) fields using a high-resolution numerical model driven by seasonal climatologies of temperature, salinity, and wind stress. The in situ 3-D temperature and salinity climatologies were calculated from the available archive of CTD, XBT, and ARGO hydrographic data. The mean wind fields are from the NCEP reanalysis. Their average summer mean DOT field is shown in Fig. 16.12. No altimeter data are used in their model calculation.

Comparisons between their dynamic topography fields and those from JPL and AVISO (incorporating altimeter and satellite gravity measurements) showed reasonable agreement

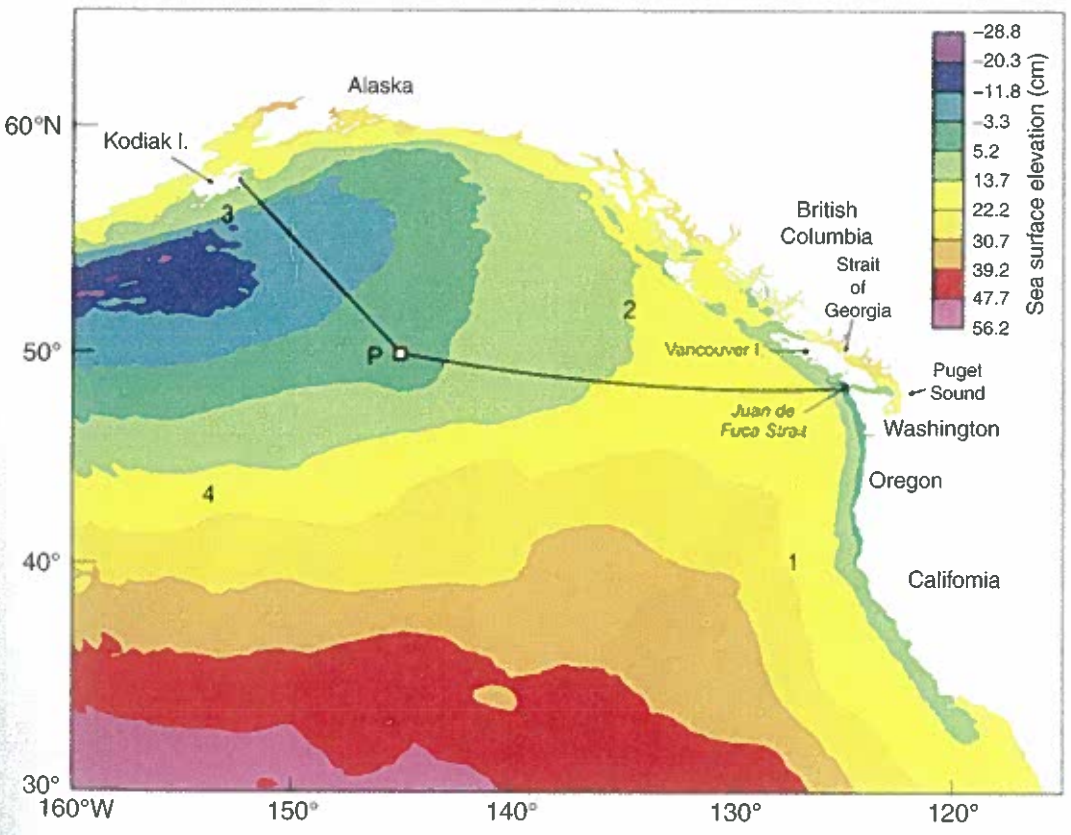

Fig. 16.12 Average summer mean dynamic topography (cm) computed from temperature and salinity climatology and NCEP wind stress. Consistent with T/P and Jason altimeter data the white square at the location of former weather station PAPA; the elevation is adjusted to have a value of 3.15 cm (Foreman et al. 2008)

in the deep ocean and poor agreement over the continental margins, within approximately 500 km of land. Their model compared well with alongtrack altimeter SSH differences near the margins, especially in the 200 km next to land where model and altimeter data show strong features (10–15 cm changes). Comparisons between the model and coastal tide gauge measurements were also good. The importance of this study for coastal analysis lies in the fact that models of this type could be run with very high resolution and extended into the 50 km next to the coast. They would then provide an absolute mean SSH field to replace the missing temporal mean in altimeter time series, resulting in time-variable fields of absolute SSH and currents in coastal domains.

Considering interannual time scales, Strub and James (2002b, c) used gridded and alongtrack altimeter data to describe the paths by which anomalous ocean conditions appeared along the mid-latitude west coasts of both North and South America (Strub and James 2002b, c) during the 1997–1998 El Niño. SSH data from the T/P tracks within ~100 km of the coast were used as proxy tide gauge data over the path between the equator and the mid-latitudes in both hemispheres, allowing lagged correlations between SSH at different locations, along with correlations between SSH and local winds to separate distant and local forcing effects. The results show that SSH signals traveled quickly down the coast of South America in May 1997. Off North America, large-scale signals traveled between the equator and the mouth of the Gulf of California (22°N) in May, and then slowly filled the Gulf until July–August, when they continued up the coast of North America (Fig. 16.13).

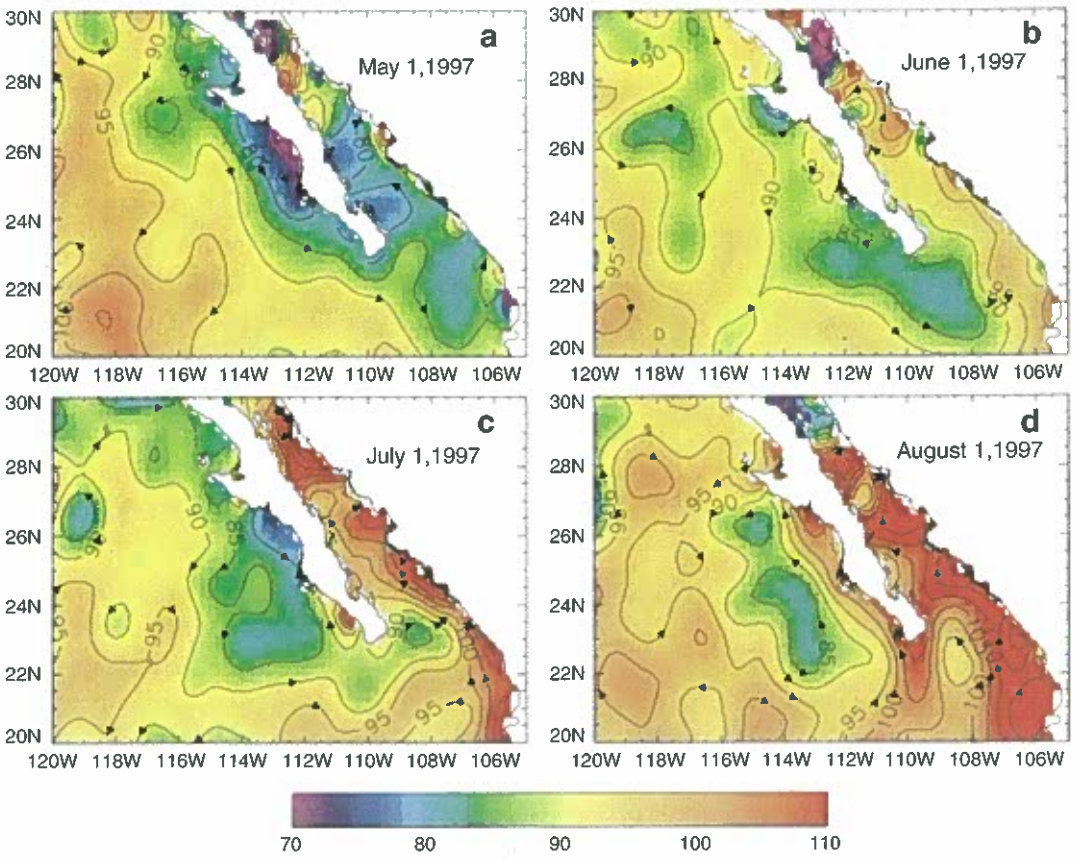

Fig. 16.13 Individual 35-day snapshots of SSH around the mouth of the Gulf of California and southern Baja California during May-August, 1997 (Strub and James 2002b)

This was not accomplished by classical "Kelvin wave" dynamics, but by a more advective process, by which they filled the mouth of the Gulf and created an artificial "coast" of high SSH, which allowed the northward movement to continue. North of 30°N, local fall and winter winds became more important in forcing the SSH anomalies, becoming the dominant factor off British Columbia and Alaska.

With the availability of gridded, multi-satellite altimeter SSH and velocity fields from the AVISO project, produced by SSALTO/DUACS, it has become less common for individual investigators to grid their own alongtrack data. The AVISO data do not incorporate tide gauge data, since they are global in scope, and do not accurately represent the region within 50 km of the coast as mentioned earlier. Even when investigators regrid the along-track data for a specific study, tide gauge data are often not available. For example, when Espinosa-Carréon et al. (2004) show seasonal and non-seasonal EOF's of SSH, SST, and satellite surface chlorophyll (CHL) off Baja California, most of the information in the 50–100 km next to the coast is provided by the SST and CHL. The SSH fields are more useful in describing the mesoscale circulation in the 500 km next to the coast. Off Oregon and Washington, Venegas et al. (2008) present similar seasonal and non-seasonal fields of SSH, SST, CHL, and surface winds, which extend over the narrow (20–50 km) shelf. One must realize, however, that both altimeter and scatterometer are extrapolated into the 30–50 km region next to the coast. The interpretation of the nearshore SSH fields is aided, in this study, by the SST data, with much higher spatial resolution and a close relation to the SSH data. This brings out both the limitations of the altimeter and the utility of multi-sensor analyzes in coastal ocean studies.

Even with the inclusion of TG SSH, the gridded SSH fields cannot resolve the smaller eddies (tens of kilometers) found next to the coast. This can be seen in Fig. 16.10 (right), where contours of gridded SSH are overlain on an SST field (Strub and James, 1997, unpublished). The SSH field provides reasonable representation of the meandering jet and associated eddies at distances of 100 km from the coast and with scales of approximately 100 km or more. It misplaces some of the eddies, as Pascual et al. (2006) have shown is the case when less than four altimeters are used, but the combination of SST and SSH provides a realistic view of the mesoscale circulation field. However there is a smaller (10–30 km) cyclonic eddy, next to the coast in the SE part of the field that cannot be resolved by the gridded field. This is typical of most comparisons between SST and SSH fields examined in this region and raises the question of whether there is additional information from the alongtrack altimeter data that could be used on smaller scales, next to the coast. It also reinforces the benefit of combining SSH data with SST fields, especially in upwelling regions where the SST fields serve as a proxy (albeit imperfect) for SSH.

One of the few attempts to look in detail at the SSH data along tracks approaching the coast of North America is reported by Saraceno et al. (2008), who investigated tracks off Northern California, Oregon, and Washington. Fig. 16.14 shows SSH data along two tracks approaching the Oregon coast (both ascending and descending T/P and Jason tracks approach the coast off the U.S. west coast), overlaid from a coincident SST image.

Standard along-track altimeter data are flagged as unreliable east of the cross-over, 50–60 km from the coast. In this case, we have simply replaced the wet tropospheric correction from the onboard radiometer with an estimate of the correction from the ECMWF atmospheric model water vapor field. Although the model correction is overly smooth, it allows us to see the

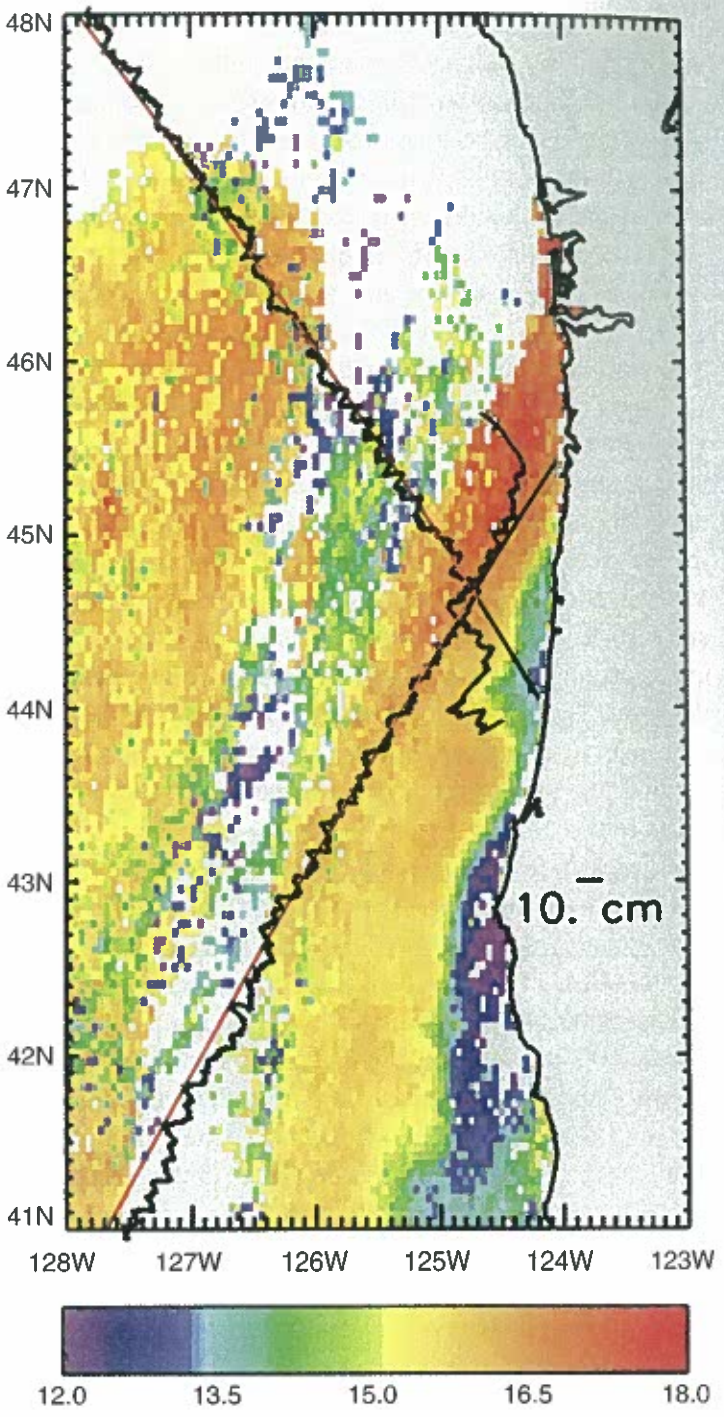

Fig. 16.14 SST (colors) and alongtrack SSH from the Jason-1 altimeter during June 27–29, 2005. Clouds are indicated by gray or speckled patterns in SST. Altimeter tracks are the "straight" lines and SSH is shown as a line plot "above" (east) or "below" (west) the tracks. Sharp drops in SSH (13 cm and 25 cm) are seen along the track moving from NW to SE, as it approaches the coast and passes over recently upwelled, colder, and denser water (Saraceno et al. 2008)

sharp drops in SSH along the track the moves from the NW to the SE, as the track moves over two fronts, one hidden by an upper layer of warm water and the second clearly visible in the SST field. Closer to the coast, other corrections (tides, tracking) eliminate the data at distances of approximately 20 km from the coast. The challenge is to first retrieve the along-track SSH data and then to use it in a realistic fashion to improve SSH fields next to the coast. Tracks are separated by distances and times too great to resolve the rapidly changing small spatial scales

of coastal features. Use of the alongtrack data where and when it is sampled is one option, combining with SST and surface color satellite fields or in situ data. Assimilation into coastal circulation models is the other approach under investigation.

16.4.1.1 Ageostrophic Currents in the California Current System

One of the more difficult problems in an eastern boundary current region like the California Current is estimating the ageostrophic component of the current. Since the altimeter cannot measure this component of the current the approach here was to have an independent measure of the total current and subtract off the geostrophic current as estimated from the coincident altimeter data. Total currents were computed both from drifting buoys and infrared and ocean color satellite imagery (Matthews and Emery 2009). Data from Jan. 1994 to December, 2005 were used in this study and Fig. 16.7 shows a comparison between these three different types of current estimators for four fall examples in the central California Current region (between San Francisco and Los Angeles). During this time three satellite altimeters were operating (ERS-1, ERS-2, and T/P). The altimetry derived geostrophic currents are mapped as green, the image-derived currents by red, and the drifting buoy currents are in blue.

Throughout the sequence, the meander offshore of Point Reyes closes off to form a zonally elongated cyclonic eddy, while the alongshore jet is displaced westward. Closer examination of the coincident MCC (called MCC currents for the maximum cross-correlation method used to compute them) and altimetry observations shows a steady westward displacement of the MCC velocities relative to the geostrophic flow. The strong offshore current, relative to the geostrophic flow, suggests that a shallow locally wind driven current is possibly being measured by the MCC method.

This example time series demonstrates the close correlation between the image derived currents and those from the trajectories of the drifting buoys while the geostrophic currents computed from the altimeter data often agree but also exhibit places when they do not agree at all. These are likely instances of strong ageostrophic flow in this strongly wind-driven coastal region.

Time averaged MCC currents exhibit strong offshore jet-like currents extending offshore and coinciding with major topographic and coastline features such as promontories. These jets are not generally in the geostrophic altimeter currents. This suggests that these oceanic features are likely ageostrophically driven and are tied to local wind and bottom topography. In addition eddy statistics computed from the MCC velocities indicate dramatically different dynamics in the near-shore and offshore regions similar to those results discussed earlier for the California Current System. Near-shore regions show a dramatic decrease in Eddy Kinetic Energy (EKE), with major axes of variance that are modulated by the shape of the coastline. Offshore, EKE levels increase and major axes of variance are aligned in the meridional direction.

It should be observed that the mesoscale geostrophic currents depicted in particular by the satellite altimetry, is composed largely of eddies and meanders that dominate the California Current System during all seasons (Fig. 16.15).

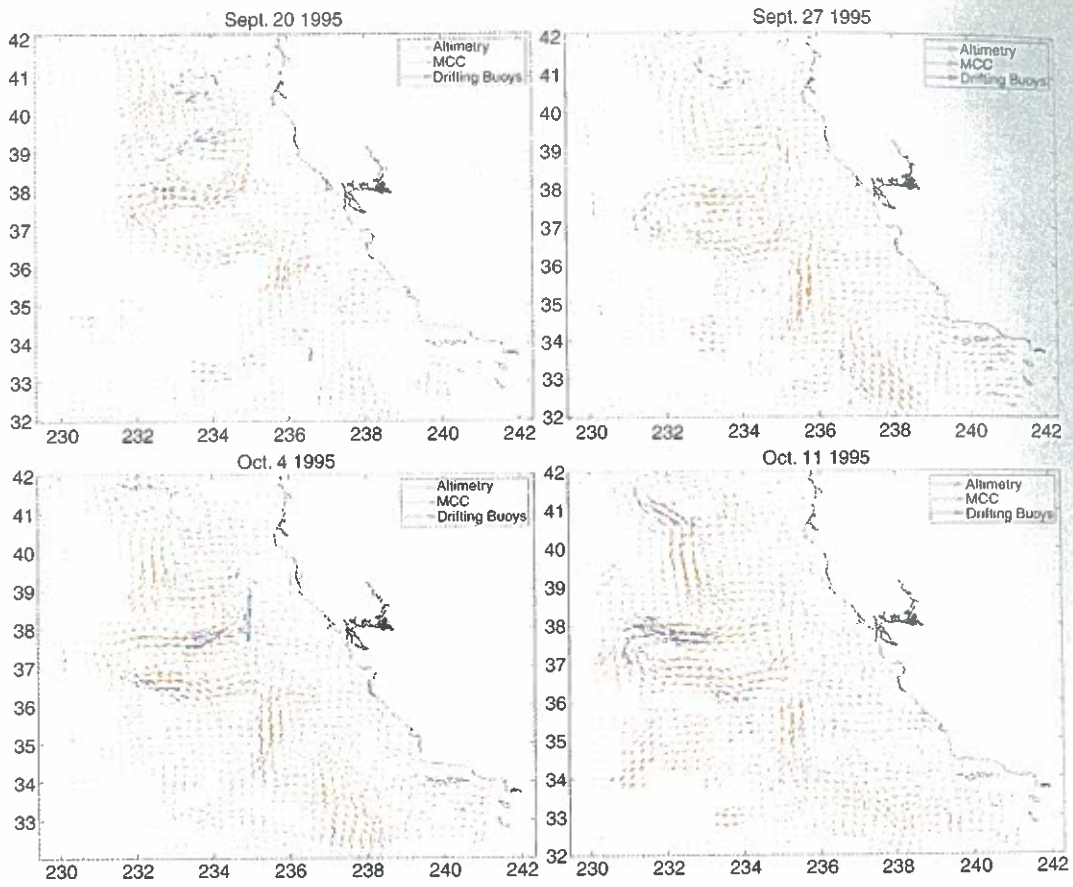

Fig. 16.15 A sample time series of current fields from satellite altimetry (*green*), drifting buoys (*blue*) and infrared + ocean color sequential images (red) using data from Sept. 20, 1995 to Oct. 11, 1995 (Matthews and Emery 2009)

All the different current observation methods exhibit clearly this mesoscale circulation structure. So these mesoscale features are characteristic both of a western boundary current region such as the Gulf Stream and an eastern boundary current region such as the California Current System. They are rather ubiquitous features whenever there is a moderately strong ocean surface current.

16.4.1.2 Numerical Modeling of the Structure and Dynamics of the California Current System

The mesoscale variability in the California Current System was modeled by Marchesiello et al. (2003) using the Regional Oceanic Modeling System (ROMS) model. The model spanned the entire California Current System with a 3.5 km horizontal resolution and was forced by mean-seasonal momentum, heat and water fluxes at the surface, and adaptive nudging to gyre-scale fields at the open water boundaries. The model equilibrium solutions show realistic mean and seasonal conditions of vigorous mesoscale eddies, fronts, and filaments.

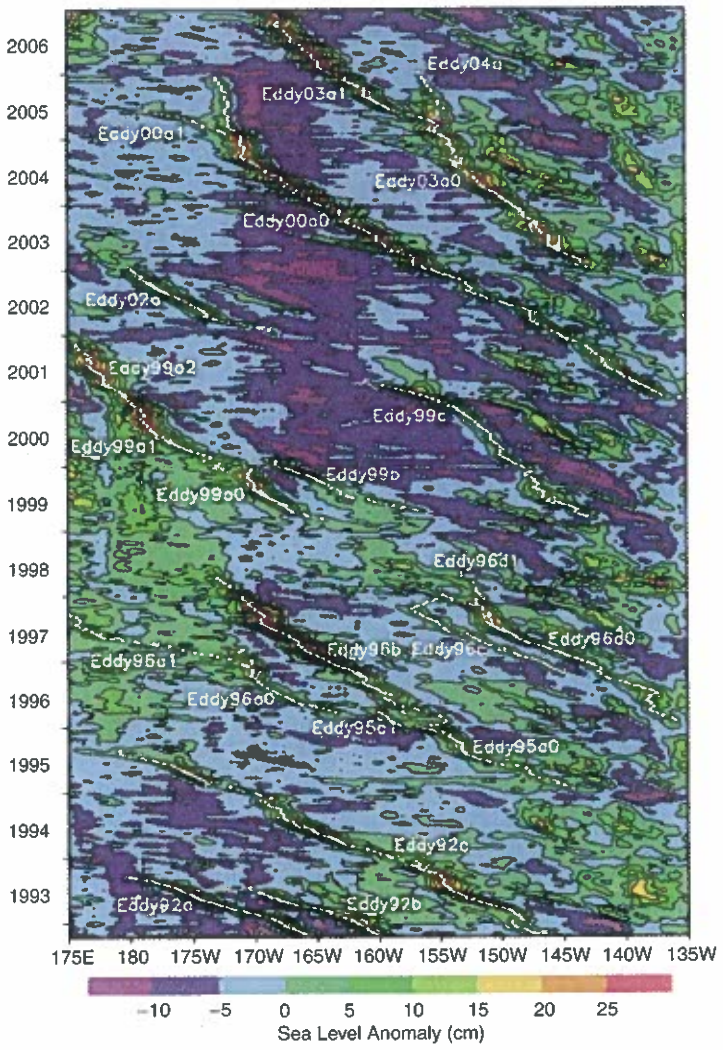

Fig. 16.16 Longitude-time (Hovmueller) diagram of the sea level anomaly (SLA) along the northern boundary of the Pacific. The SLA was averaged within 2° south of the 1,000 m depth contour (Ueno et al. 2009)

Seasonal variations of model sea surface height (SSH) from both northern and southern latitudes are plotted along with that from the T/P altimeter and the alongshore wind stress in Fig. 16.20. The maximum in wind-driven upwelling season is in summer in the northern region but earlier in spring off California (consistent with observations discussed by Strub and James 2000). Model and altimeter data both show nearly coincident wind and oceanic response suggesting that the coastal seasonal cycle is locally forced with no evident oceanic teleconnections between southern and northern regions.

The seasonal westward propagation in the upwelling region of the California Current System is demonstrated in Fig. 16.21 for both the SSH (left panel) and for surface and depth-integrated Eddy Kinetic Energy (EKE). Extrema in all these three quantities move offshore at a speed of about 2 cm/s in quasi-recurrent seasonal patterns. This is the speed that would be expected from baroclinic Rossby waves as pointed out for this region in observational studies (Kelly et al. 1998; Chelton and Schlax 2007).

The primary eddy generation mechanism is the baroclinic instability of upwelling, alongshore currents. There is a progressive movement of mean-seasonal currents and eddy energy offshore and downward into the oceanic interior in an annually recurrent cycle.

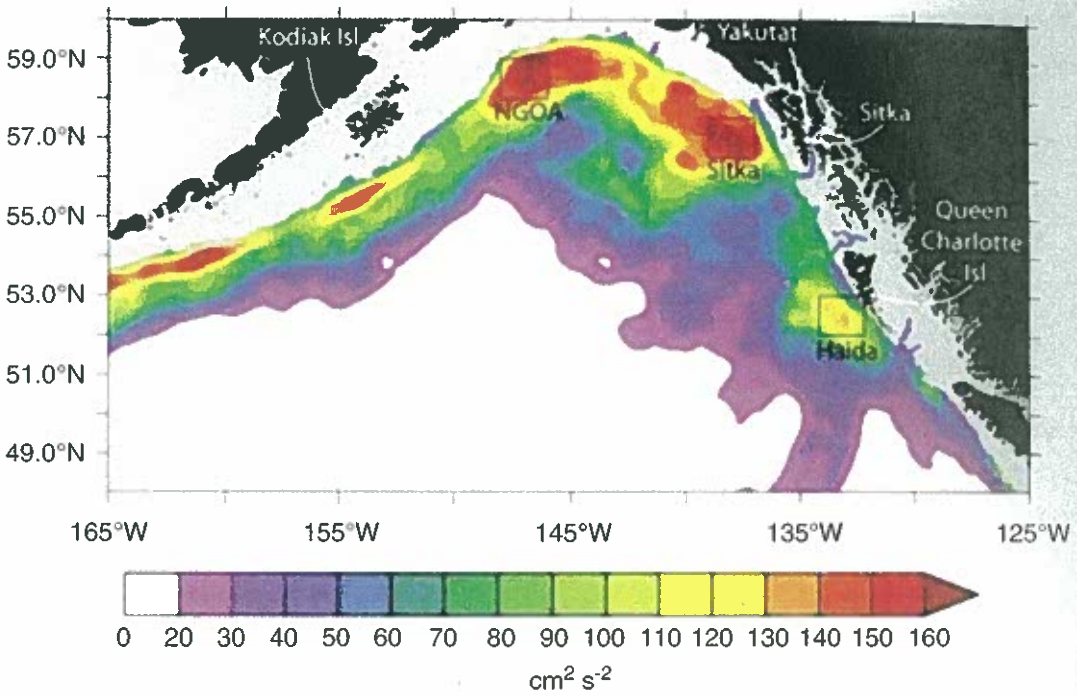

Fig. 16.17 Mean Eddy Kinetic Energy ($cm^2\ s^{-2}$). Gray region is the continental shelf (<300 m depth. Ladd 2007)

16.4.1.3
Numerical Modeling of the Southern California Bight and Comparisons with Satellite Altimetry Data

The circulation in the Southern California Bight (SCB) is influenced by the background California Current farther offshore, by tropical remote forcing through the coastal waveguide alongshore, and local atmospheric forcing. The region is characterized by local complexity in its topography and the coastline. ROMS is applied to the SCB circulation, its multiple-scale variability, and interannual, seasonal, and intraseasonal variations. Three nested horizontal grid resolutions of 20, 6.7, and 1 km are forced with momentum, heat, and freshwater fluxes at the surface and nudging to gyre-scale reanalysis fields at the boundaries. This oceanic model starts in an equilibrium state from a multiple-year cyclical climatology run and is integrated from 1996 to 2003. The 1 km resolution results are compared against HR radar data, current meters, ADCP) data, hydrographic measurements, tide gauges, drifting buoy trajectories, satellite altimeter currents, and satellite radiometer data. T/P SSHA data are used to assess the low-frequency variability in the ROMS model simulation of the SCB circulation. One altimeter pass through the 1 km SCB model domain (Fig. 16.22) which are labeled as Lines 43, 199, and 206; this altimeter data paucity is why these authors decided not to compare their model outputs with any of the gridded altimeter products. SSH anomalies from these three ground tracks are plotted in Fig. 16.23 for both the T/P observations and for the ROMS model simulations. The T/P data are 10-day SSH anomalies relative to a 9 year (1993–2001) mean sea surface. Fortunately the 1997–1998 ENSO event is contained within this short time series. ROMS SSH anomalies are also referenced to the same 9-year mean sea surface. There are clear interannual events that are

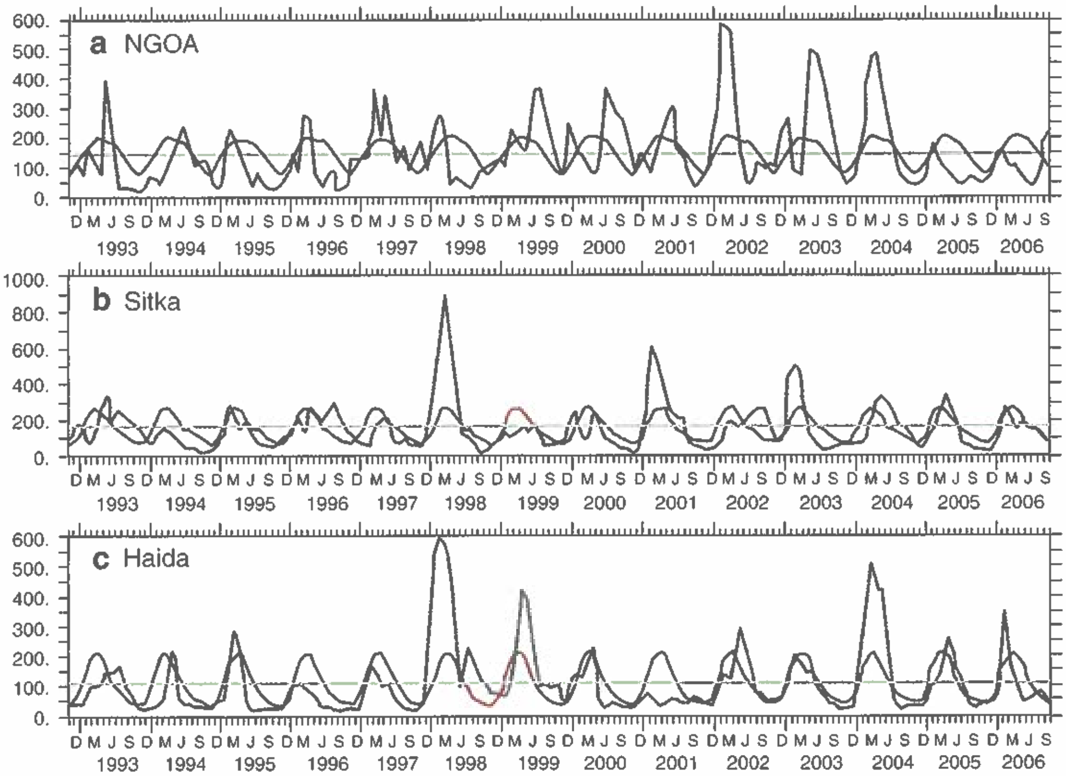

Fig. 16.18 Time series of monthly averaged (*black*), monthly climatological mean (*red*), and mean (*green*) EKE (cm^2/s^2) averaged over the areas around Kodiak (**a**), Sitka (**b**), and Haida (**c**) (Ladd 2007)

coherent between the tracks and often between T/P and ROMS. One that is not even coherent is in late 2000 when a low-SSH in T/P is not matched in ROMS. The largest positive SSH anomalies are during 1997–1998 in both T/P and ROMS. The ROMS anomalies are only slightly larger than the T/P data.

16.5 Alaskan Stream

Eddies also dominate the Alaskan Stream region (Ueno et al. 2009) again reflected in satellite altimetry data between 1992 and 2006 and profiling float data. Fifteen long-lived eddies were identified and tracked during their westward migration through the North Pacific (Fig. 16.16).

Of these, three eddies were present at the start of the satellite altimetry observations, three formed in the eastern Gulf of Alaska off Sitka, Alaska, and four were first detected at the head of the Gulf of Alaska near Yakutat, Alaska. The other five eddies formed along a line between 157° and 169°W. Most of the eddies formed in the Gulf of Alaska decayed before exiting the Gulf while those eddies formed farther south managed to cross 180° reaching the western subarctic gyre. Four of the five-southern eddies formed under negative or weakly positive wind stress curls. Comparison of the southern eddy propagation with the local bottom topography suggests that eddies propagated faster over steeper

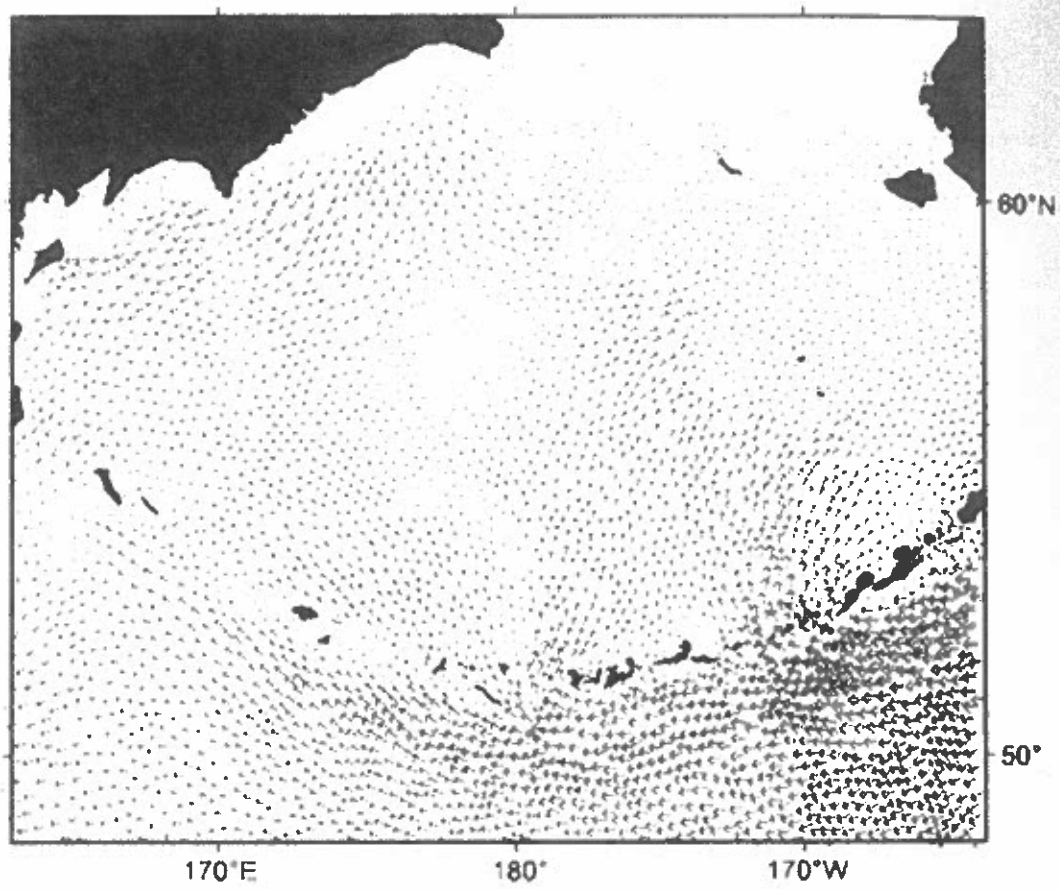

Fig. 16.19 Vertically integrated energy flux for M_2 (post assimilation). Each full shaft in a multi-shafted vector represents 100 KW/m. The latitudinal scale has been selected and vectors have been sub-sampled so that the minimum separation is 20 km (Foreman et al. 2006)

bottom slopes although eddy speeds observed were slower than those predicted by the topographic planetary wave dispersion relation.

In a related study Ladd (2007) used satellite altimetry data to map eddy kinetic energy in the Gulf of Alaska (Fig. 16.17).

High EKE is associated with the Alaskan Stream which is seen as a narrow structure of high EKE that reflects and strongest and most unstable component of the circulation in the Gulf of Alaska. Note the pockets of high EKE in the waters surrounding Kodiak, Sitka, and Haida (Queen Charlotte Islands). Of these the Sitka and Haida are eddy formation regions while the area around Kodiak is an area through which all eddies formed in the eastern Gulf of Alaska are forced to pass and interact with bottom and coastal topography. Thus, the variability in the Sitka and Haida regions is due to the formation of mesoscale eddies and the variability at Kodiak is due to the passage of mesocale eddies formed farther to the east. The SLA pattern at Sitka suggests that eddies form here, flow seaward then turn northward in the northwestward flowing Alaska Current. Eddies formed in the Haida region do not move as much offshore and appear to simply advect to the north.

Time series of monthly averaged (black) EKE's at these three locations exhibit a very clear climatological mean signal that has a maximum in March and minimum in November (Fig. 16.18).

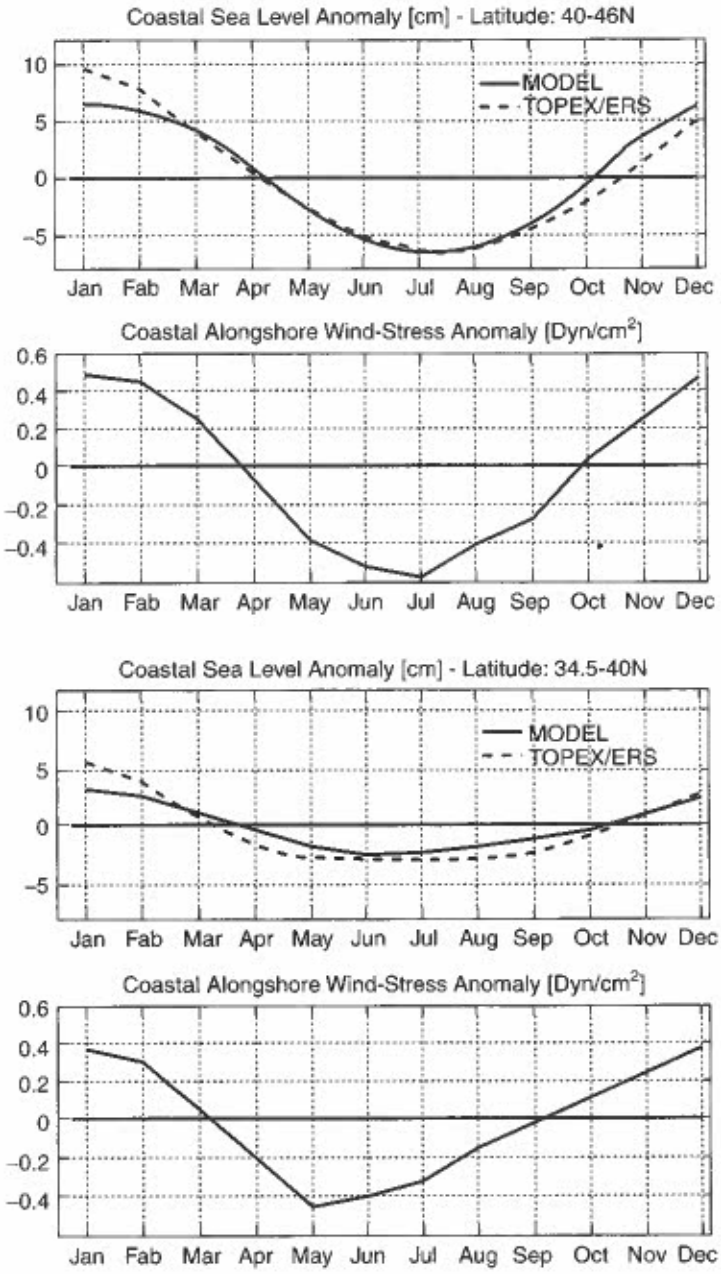

Fig. 16.20 Near-shore seasonal cycle of simulated and T/P and ERS SSH anomalies and alongshore wind stress. The variables are averaged over 100 km wide alongshore strips (*top*) between 40° and 46°N and (*bottom*) between 34.5° and 40°N (Marchesiello et al. 2003)

Maximum EKE occurs as the downwelling winds start to weaken. The strong downwelling favorable winds in December/January drive a coastal current flowing northwest with associated cross-shelf density gradients and storage of potential energy. As these winds weaken periods of upwelling favorable winds become more likely. These wind driven events convert this potential energy to kinetic energy through baroclinic instability (Ikeda et al. 1986).

These time series also clearly indicate the effects of El Nino on the altimeter derived EKE. There are however, some weaker El Nino events that do not show up in these time series. The black monthly averaged line in Fig. 16.19 exhibits a peak at the 1997–1998 El Nino event. It is interesting that this peak is present at Haida and Sitka but by the time the SLA had reached the Kodiak region the El Nino signal had dissipated.

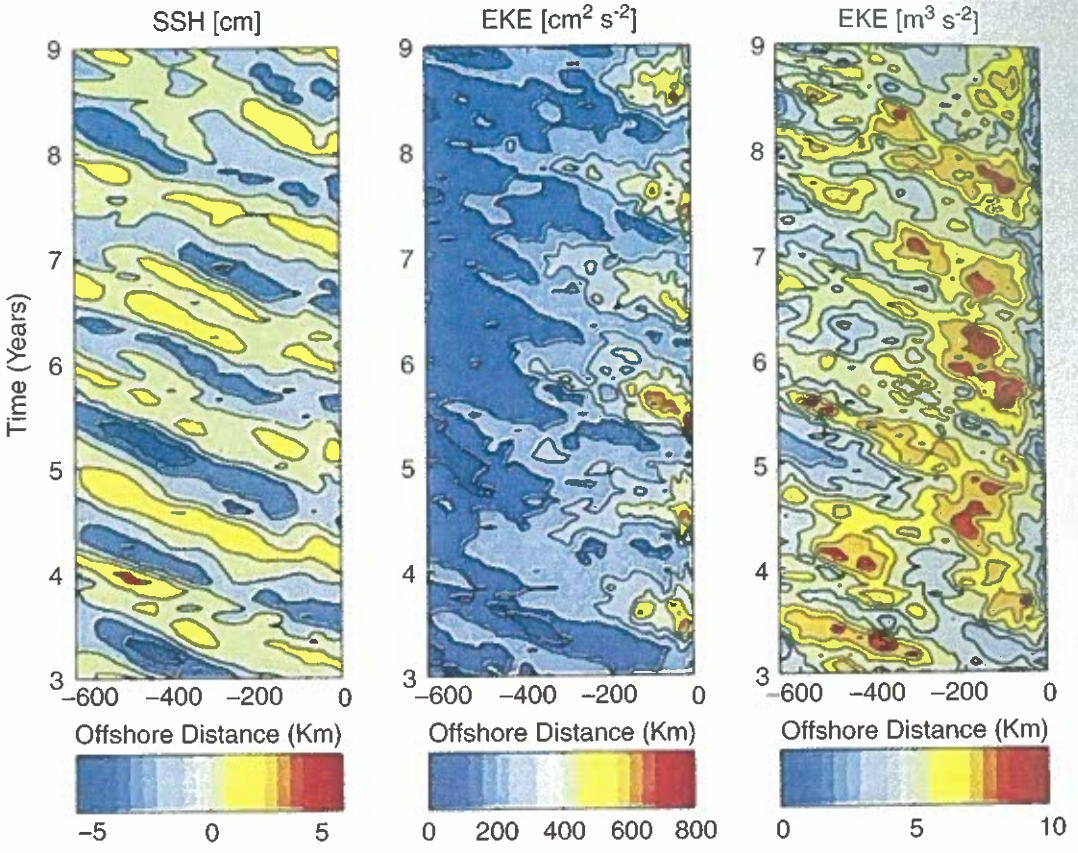

Fig. 16.21 Hovmoeller plots for SSH anomalies (CI = 2 cm), surface EKE (CI = 100 cm²/s²), and depth-integrated EKE (CI=1 m³s⁻²) from the model with 5 km resolution and averaged alongshore in the upwelling region (34.5°–43°N; Marchesiello et al. 2003)

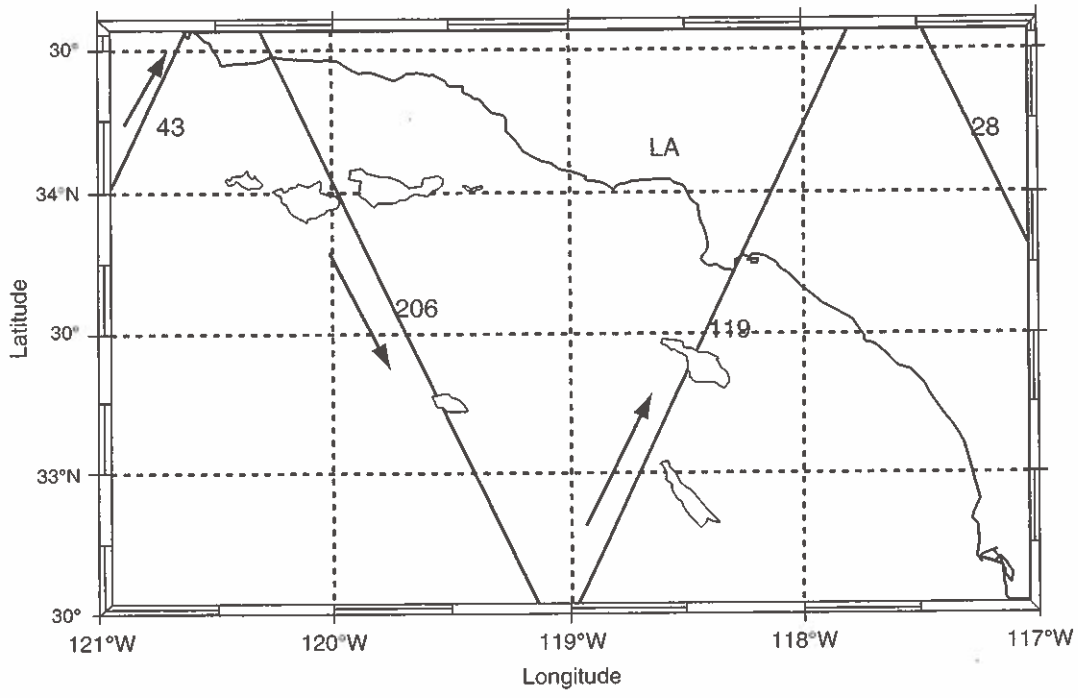

Fig. 16.22 T/P satellite tracks over the SCB. The arrows are the direction the satellite moves along the track (Marchesiello et al. 2003)

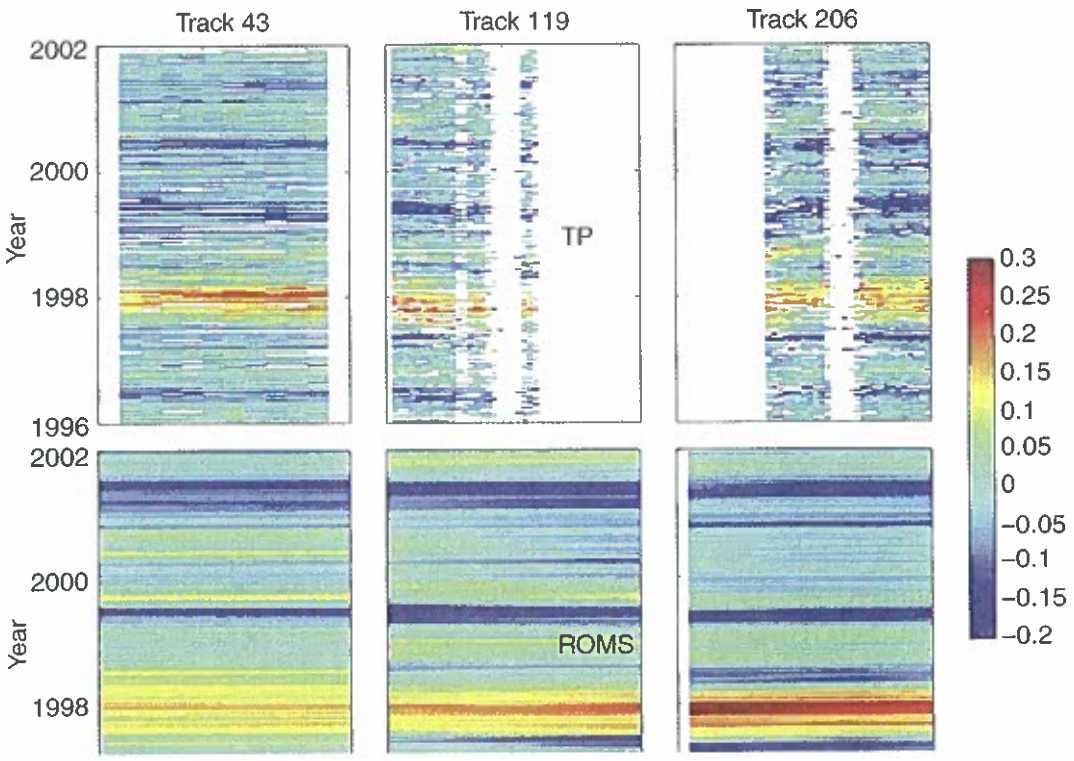

Fig. 16.23 Along-track SSH anomalies (m) from T/P (*top row*) and ROMS (*bottom row*), each relative to its own time and track mean. The distance on the abscissa starts from the beginning point of a track in the domain (Fig. 16.22; Marchesiello et al. 2003)

16.6 Tidal Energy in the Bering Sea

Although unresolved tidal motions limit the use of altimetry in coastal regions over shallow continental shelves, tides and their energy also represent important oceanographic processes for mixing and transport. Thus, the generation of strong tidal motions by topographic features in shallow regions and the propagations of that energy along the coast or into the deep ocean is a topic of interest in coastal oceanography. Combinations of tidal models and altimeter measurements have proved useful in studying the flux of tidal energy, as demonstrated by Foreman et al. (2006). In this case, tidal harmonics are computed from T/P altimetry and assimilated into a barotropic, finite element model of the Bering Sea and its boundaries. After evaluating its accuracy through comparisons with independent bottom pressure gauges, the model is used to estimate energy fluxes through each of the Aleutian Passes and the Bering Strait and to construct an energy budget for the major tidal constituents. The finite element model does not conserve mass locally and this gives rise to an additional error term in the energy budget, whose contribution is significant for the model prior to assimilation but is reduced substantially with the assimilation technique.

The M_2 tidal constituent is estimated to have the largest net energy flux into the Bering Sea but the sum of the first three largest diurnal constituents is found to be greater than the sum of the largest three semi-diurnals. The vertically integrated energy flux for the M_2 tide

is presented here in Fig. 16.19 as a case after altimeter data assimilation. Samalga and Amutka Passes in the Aleutians are found to be the primary conduits for the influx of semi-diurnal energy while Amchitka Pass is the primary conduit for diurnal energy. A significant portion of the diurnal energy is seen to exist in the form of continental shelf waves trapped along Bering Sea slopes.

16.7 Future Work

Most of the problems facing coastal oceanography off North America are common to other regions in the world. First the nature of the altimeter waveforms in the coastal ocean need to be investigated and a retracking method selected and implemented. It is widely accepted that the last 10 km close to the shore requires retracking of the altimeter waveform. Retracked altimetry needs to be compared with higher resolution coastlines and land digital elevation models (DEM's). It is not clear that there is one single retracking method that will be useful in all regions. Instead the retracking method may vary with geographic location as the fairly narrow shelf of the west coast may not impact the altimeter waveform too greatly while the much wider shelf off the east coast may contribute to changes in the altimeter waveforms that have to be corrected. It is important that these corrections be developed to the best of our ability because the coastal zone is where the bottom topography changes very rapidly.

The atmospheric moisture correction for the altimeter path-length is also a problem in the coastal ocean where the large spot sizes of the passive microwave radiometers are easily contaminated by land and restrict their utility to farther offshore than many coastal oceans. Many land decontamination methods have been recently developed and used to reprocess earlier altimeter data. It is difficult to evaluate these reprocessed water vapor data as there are few independent direct measurements of atmospheric water vapor in the coastal atmosphere. Improvements have been and are being made to the passive microwave radiometers to increase spatial resolution making it possible to bring this measurement closer to the coast. Still there is need to continually improve the water vapor corrections in the coastal zone. Finally there is real need to get the tidal corrections very precise in the coastal zone as here the tidally forced currents can become non-linear and difficult to forecast. Thus, we need the best possible calibration/validation systems to provide corrections to the altimeter data in the dramatic space/time variability in the coastal zone such as that carried out by Liu and Weisberg (2007) for the West Florida coast.

References

Badan-Dangon A (1998) Coastal circulation from the Gal´apagos to the Gulf of California. In: Robinson A, Brink KH (eds) The sea, vol 11, pp 315–343

Bograd SJ, Lynn RJ (2003) Long-term variability is the southern California current system. Deep-Sea Res II 50:2355–2370

Bograd SJ, Thomson RE, Rabinovich AB, LeBlond PH (1999) Near-surface circulation of the northeast Pacific Ocean derived from WOCE-SVP satellite-tracked drifters. Deep-Sea Res II 46:2371–2403

Boicourt WC, Wiseman WJ, Valle-Levinson A, Atkinson LP (1998) Continental shelf of the southeastern United States and the Gulf of Mexico: in the shadow of the western boundary current. In: Robinson AR, Brink KH (eds) The sea, vol II: the global coastal ocean-regional studies and syntheses. Wiley, New York, pp 135–182

Carton JA, Chao Y (1999) Caribbean Sea eddies inferred from TOPEX/Poseidon altimetry and a 1/6° Atlantic Ocean model simulation. J Geophys Res 104:7743–7752

Chelton DB, Schlax MG, Samelson RM, de Szoeke RA (2007) Global observations of large oceanic eddies. Geophys Res Lett 34:L15606. doi:10.1029/2007GL030812

Chereskin TK, Morris MY, Niiler PP, Kosro PM, Smith RL, Ramp SR, Collins CA, Musgrave DL (2000) Spatial and temporal characteristics of the mesoscale circulation of the California current from eddy-resolving moored and shipboard measurements. J Geophys Res 105:1245–1269

Dong S, Kelly KA (2003) Seasonal and interannual variations in geostrophic velocity in the Middle Atlantic Bight. J Geophys Res 108(C6):3172. doi:10.1029/2002JC001357

Emery WJ, Thomas AC, Collins MJ, Crawford WR, Mackas DL (1986) An objective procedure to compute advection from sequential infrared satellite images. J Geophys Res 91(color issue): 865–879

Espinosa-Carréon TL, Strub PT, Beier E, Ocampo-Torres F, Gaxiola-Castro G (2004) Seasonal and interannual variability of satellite-derived chlorophyll pigment, surface height and temperature off Baja California. J Geophys Res 109:C03039

Foreman MGG, Cummins PF, Cherniawsky JY, Stabeno P (2006) Tidal energy in the Bering Sea. J Mar Res 6:797–818

Foreman MGG, Crawford WR, Cherniawsky JY, Galbraith J (2008) Dynamic ocean topography for the northeast Pacific and its continental margins. Geophys Res Lett 35:L22606. doi: 10.1029/2008GL035152

Freeland HJ, Gatien G, Huyer A, Smith RL (2003) Cold halocline in the northern California current: an invasion of subarctic water. Geophys Res Lett 30(3):114L

Han G (2004) Scotian Slope circulation and eddy variability from TOPEX/Poseidon and frontal analysis data. J Geophys Res 109:C03028. doi:10.1029/2003JC002046

Han G (2007) Satellite observations of seasonal and interannual changes of sea level and currents over the Scotian Slope. J Phys Oceanogr 37:1051–1065. doi:10.1175/JPO3036.1

Han G, Tang CL (2001) Interannual variations of volume transport in the western Labrador Sea based on TOPEX/Poseidon and WOCE data. J Phys Oceanogr 1:199–211

Han G, Hannah CG, Smith PC, Loder JW (1997) Seasonal variation of the three-dimensional circulation over the Scotian Shelf. J Geophys Res 102:1011–1025

Haney RL, Hale RA, Dietrich DE (2001) Offshore propagation of eddy kinetic energy in the California current. J Geophys Res 106:11,709–11,717

Hickey BM (1998) Coastal oceanography of western North America from the tip of Baja California to Vancouver Island. In: Robinson AR, Brink KH (eds) The sea, Vol 11. Wiley, New York

Ikeda M, Emery WJ, Mysak LA (1986) Seasonal variability of the meanders in the California current system off Vancouver Island. J Geophys Res 89:3487–3505

Keister JE, Strub PT (2008) Spatial and interannual variability in mesoscale circulation in the northern California current system. J Geophys Res 113:C04015. doi:10.1029/2007JC004256

Kelly KA (1989) An inverse model for near-surface velocity from infrared images. J Phys Oceanogr 19:1845–1864

Kelly KA, Gille ST (1990) Gulf Stream surface transport and statistics at 69°W from the Geosat altimeter. J Geophys Res 95:3149–3161

Kelly KA, Strub PT (1992) Comparison of velocity estimates from advanced very high resolution radiometer in the coastal transition zone. J Geophys Res 97(C6):9653–9668

Kelley KA, Beardsley RC, Limeburner R, Brink KH, Paduan JD, Chereskin TK (1998) Variability of the near-surface eddy kinetic energy in the California Current based on altimeter, drifter and moored current meter data. J Geophys Res 103:13067–13083

Ladd C (2007) Interannual variability of the Gulf of Alaska eddy field. Geophys Res Lett 34:L11605. doi:10.1029/2007GL029478

Leben RR (2005) Altimeter-derived loop current metrics. In: Sturges W, Lugo-Fernandez A (eds) Circulation in the Gulf of Mexico: observations and models. AGU Geophys Monograph, vol 161, pp 181–202

Le Traon PY, Faugere Y, Hernandez F, Dorandeu J, Merttz F, Ablain M (2003) Can we merge GEOSAT-follow-on with TOPEX/Poseidon and ERS-2 for an improved description of the océan circulation? J Atmos Oceanic Technol 20:889–895

Liu Y, Weisberg RH (2007) Ocean currents and sea surface heights estimated across the West Florida Shelf. J Phys Oceanogr 37:1697–1713

Loder JW, Boicourt WC, Simpson JH (1998) Overview of western océan boundary shelves. The Sea, vol 11. Wiley, New York

Lohrenz SE, Verity PG (2006) Regional oceanography: Southeastern United States and Gulf of Mexico. In: Robinson AR, Brink KH (eds), The Sea, Vol 13, Wiley, New York

Mackas DL, Peterson WT, Ohman MD, Lavanlegos BE (2006) Zooplankton anomalies in the California current system before and during the warm ocean conditions of 2005. Geophys Res Lett 33:L22S07. doi:10.1029/2006GL027930

Marchesiello P, McWilliams JC, Shchepetkin AF (2003) Equilibrium structure and dynamics of the California current system. J Phys Oceanogr 33:753–783

Matthews DK, Emery WJ (2009) Velocity observations of the California current derived from satellite imagery. J Geophys Res 114:C08001. doi:10.1029/2008JC005029

Mooers CNK, Maul GA (1998) Intra-Americas Sea coastal ocean circulation. In: Robinson AR, Brink KH (eds) Global coastal ocean. The sea, vol 11, Wiley, New York, pp 183–208

Pascual A, Gaugere Y, Larnicol G, Le Traon PY (2006) Improved description of the ocean mesoscale variability by combining four satellite altimeters. Geophys Res Lett 33:L02611. doi:10.1029/2005GL024633

Royer TC (1998) Coastal processes in the northern North Pacific. In: Robinson AR, Brink KH (eds) The sea, vol 11, chap 13, pp 395–414. Wiley, New York, 1062 p

Saraceno M, Strub PT, Kosro PM (2008) Estimates of sea surface height and near-surface alongshore coastal currents from combinations of altimeters and tide gauges. J Geophys Res 113: C11013. doi:10.1029/2008JC004756

Stabeno PJ, Bond NA, Kachel NB, Salo SA, Schumacher JD (1998) On the temporal variability of the physical environment over the south-eastern Bering Sea. Fisheries-Oceanogr 10:81–98

Strub PT, James C (1995) The large-scale summer circulation of the California current. Geophys Res Lett 22:207–210

Strub PT, James C (2000) Altimeter-derived variability of surface velocities in the California currne system: 2. Seasonal circulation and eddy statistics. Deep-Sea Res II 47:831–870

Strub PT, James C (2002a) Altimeter-derived surface circulation in the large-scale NE Pacific Gyres. Part 1: seasonal variability. Prog Oceanogr 53:163–183

Strub PT, James C (2002b) Altimeter-derived surface circulation in the large-scale NE Pacific Gyres. Part 2: 1997–1998 El Niño anomalies. Prog Oceanogr 53:185–214

Strub PT, James C (2002c) The 1997–1998 oceanic El Niño signal along the southeast and northeast Pacific boundaries – an altimetric view. Prog Oceanogr 54:439–458

Strub PT, James C (2003) Altimeter estimates of anomalous transports into the northern California current during 2000–2002. Geophys Res Lett 30(15):8025. doi:10.1029/2003GL017513

Strub PT, Chereskin TK, Niiler PP, James C, Levine MD (1997) Altimeter-derived variability of surface velocities in the California current system: 1. Evaluation of TOPEX altimeter velocity resolution. J Geophys Res 102:12727–12748

Sturges W, Leben RR (2000) Frequency of ring separations from the loop current in the Gulf of Mexico: a revised estimate. J Phys Oceanogr 30:1814–1819

Townsend D, Thomas A, Mayer L, Thomas M, Winlan J (2006) Oceanography of the northwest Atlantic Shelf, The sea: the global coastal ocean: interdisciplinary. Harvard University Press, Harvard

Ueno H, Freeland HJ, Crawford WR, Onishi H, Oka E, Sato K, Suga T (2009) Anticyclonic eddies in the Alaskan Stream. J Phys Oceanogr 00:1–18

Venegas RM, Ted Strub P, Beier E, Letelier R, Thomas AC, Cowles T, James C, Soto-Mardones L, Cabrera C (2008) Satellite-derived variability in chlorophyll, wind stress, sea surface height, and temperature in the northern California Current System. J Geophys Res 113:C03015. doi:10.1029/2007JC004481

Vignudelli S, Cipollini P, Roblou L, Lyard F, Gasparini GP, Manzella G, Astraldi M (2005) Improved satellite altimetry in coastal systems: case study of the Corsica Channel (Mediterranean Sea). Geophys Res Lett 32:L07608. doi:10.1029/2005GL022602

White WB, Tai CK, DiMento J (1990) Annual Rossby wave characteristics in the California current region from the Geosat exact repeat mission. J Phys Oceanogr 20:1297–1310